SESSION T

Laboratory Techniques In Space Environment Research

Chairman, LEONARD D JAFFE

DR. LEONARD D. JAFFE, *Chief of Materials Research, Jet Propulsion Laboratory, was born in Brooklyn, New York. He was graduated with a B.S. in Electrochemical Engineering from Massachusetts Institute of Technology in 1939, and received the M.S. in Metallurgy at MIT in 1940. Harvard University conferred the Sc. D. in Metallurgy upon him in 1947. Author of a text and numerous technical papers, Dr. Jaffe is a member of AIME, ASM, AAAS, ARS, APS, and Sigma Xi.*

63. Techniques for Achieving Steady-State Temperatures Above 1500° C

By Howard E. Martens

HOWARD E. MARTENS *is an Assistant Section Chief in the Materials and Research Section of Jet Propulsion Laboratory. Born in Bloomington, Illinois, he graduated with a B.S. in Mechanical Engineering from the California Institute of Technology in 1942.*

ABSTRACT

A description is given of various types of equipment used to reach steady-state temperatures above 1500° C. Applications and limitations of the equipment are reviewed. Among the types of equipment to be considered are resistance heating, induction heating, electron beam heating, and arc imaging heating.

INTRODUCTION

The rate of advance of our modern technology, as demonstrated throughout this conference, has been greatly accelerated by our entering the missile and rocket age, the atomic age, and now the space age. The advancements in these areas have certainly taxed the ingenuity of the engineer and the scientist. One area in which the rate of advance has been particularly rapid is that of high-temperature technology. Here, problems which have arisen are many and varied. Some of these problems are of interest primarily to the metallurgist; others relate to the ceramist, or to the chemist, or to the physicist, etc.

Since university representatives are likely to cover all possible fields of interest and since the amount of material which can be presented is limited by the space available, this presentation will have to be of a general nature. As such, it is likely that it may prove to be disappointing to some individuals; however, it is hoped that what is presented will meet the needs of the majority group interested in the field of high-temperature technology.

First, as indicated by the title, this presentation is to give consideration only to those techniques which are used to achieve steady-state temperatures as opposed to transient or short-time temperatures. Second, consideration is to be limited to temperatures above 1500°C. These limitations are in no way intended to evaluate the importance of the other areas, but are merely used as a means of restricting the area to be covered to some reasonable size.

Why are temperatures above 1500°C needed? If this question had been asked twenty-five years ago, many engineers and scientists might have strongly indicated that such temperatures would not be required, except for very special studies, for many many years to come. However, this has not proven to be the case. Rapid advancements made in the working fluid temperatures of the energy units now in use have quickly moved from the 500–1000°C temperature range of the steam and internal combustion engines, through the gas turbine, the rocket and the nuclear engine, and it is now commonplace to consider steady-state temperatures of 2500°C and above. The problems involved in consideration of such temperatures relate mainly to the fact that they are well above the

useful temperature of the commonly available engineering structural materials, and in many cases are above the melting point of any known materials. This is where the ingenuity mentioned earlier comes into the picture.

APPLICATIONS OF STEADY-STATE TEMPERATURES

Aside from the important fact that efficiency of energy conversion units can be improved by increasing the operating temperature, steady-state temperatures above 1500°C must be attained for other applications. Some of the more important applications are shown in Table 63–I.

TABLE 63–I.—*Applications of Steady-State Temperatures*

Material Production	Melting. Sintering. Hot pressing.
Material Fabrication	Forming. Joining. Heat treating.
Material Evaluation	Testing. Simulating.

Since very small percentages of the currently used materials are found in usable condition in nature, it is necessary that most materials be produced by chemical processes. Until a few years ago nearly all materials were produced by a process which involved melting or a liquid phase. As the desired usable temperature of engineering materials increased, so did the melting point. In those cases where melting was not a reasonable method of production, the cold pressing and sintering process was developed and used. In this process also, the most desirable temperature for the sintering process is generally near the melting point and thus requires steady-state high temperatures. Attempts to improve the results of the cold pressing and sintering process led to the development of the hot pressing technique, which again requires high temperatures.

The ability to produce materials which are useful at temperatures above 1500°C is of value only if such materials can then be fabricated into usable shapes. Unfortunately, it has been found that most materials with high useful temperatures also require fabrication at high temperature. This has meant that forming processes such as forging, extruding, spinning, etc., are now being carried on at temperatures above 1500°C. The complications of our present technology have dictated the need for joining of materials, which has led to the development of high-temperature brazing and welding techniques. To achieve the maximum efficiency from engineering structural materials some type of heat treating process is normally required. Here again, high temperatures are needed.

It is obvious, of course, that production and fabrication are only a part of the problem of using materials at temperatures above 1500°C. A third factor, and an important reason for needing to reach these temperatures under steady-state conditions, is to allow evaluation of the materials. It is perhaps in this area that laboratory techniques for obtaining high temperatures have been most widely used. In many instances materials which cannot be produced or fabricated on an acceptable commercial basis are put through a series of tests so as to determine engineering properties, the idea being that the results of such tests can be used to justify the development of production or fabrication processes. Closely allied to the high-temperature testing needs is the need to achieve high temperatures for the purpose of simulating an actual use condition. In general, this is more difficult to attain because of the competing processes involved. It is, however, an important laboratory technique because of the savings which result if it is successful.

METHODS OF ACHIEVING HIGH TEMPERATURES

These, then, are some of the more important uses of steady-state temperatures above 1500°C. As might be expected, the methods which can be used to achieve these temperatures are varied and complicated. Table 63–II lists the general types of equipment which can be used. The combustion types, which use gas, liquid, or solid fuel, or some mixture thereof, were among the

earliest developed, but in many applications have been replaced by more efficient methods, especially for temperatures above 1500°C.

TABLE 63–II.—*Methods of Achieving High Temperatures*

Combustion	Gas. Liquid. Solid.
Electrical	Resistance. Induction. Arc. Imaging. Electron beam.
Nuclear	

The most generally used type of equipment is, of course, electrical, and although its variations and combinations are far too numerous to be considered in detail in a presentation such as this, some of the more widely used types are listed in Table 63–II and will be discussed. (Although nuclear methods are not now fully developed, we are certainly not far from the time when it will be possible to use controlled nuclear processes as a source for steady-state high temperatures.)

Resistance heating is perhaps the most widely used of the several electrical types listed. For this equipment an element in the form of wire, ribbon, rod, or tube is heated by passing an electric current through it. The maximum temperature which can be achieved depends on the material from which the element is made, as well as the material used as insulation. Figure 63–1 shows a particular type of resistance furnace in which oxide elements are used as the primary source of temperature. It is necessary that such elements be preheated to a temperature at which they become conductive. To accomplish this, secondary heating elements are used. If the primary elements are made from materials such as metals or carbides which are conductive at room temperature, then the secondary elements can be eliminated.

There is, of course, a wide variety of materials which can be used for heating elements. However, for temperatures above 1500°C the number is quite limited. The refractory metals or alloys, the conductive oxides of zirconium, and carbon are about the only suitable materials for this temperature range.

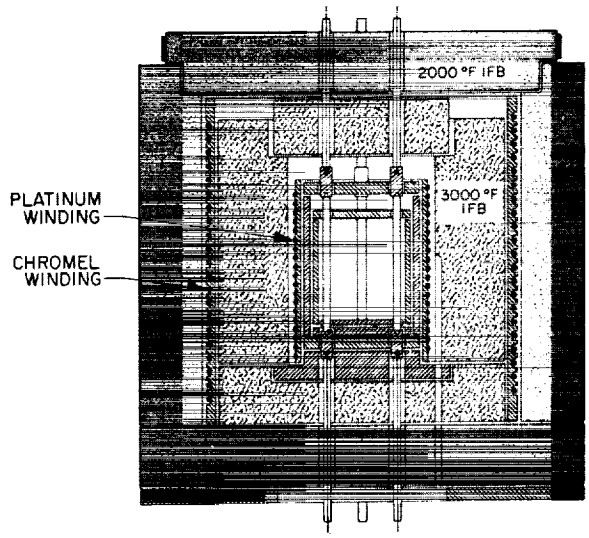

FIGURE 63–1.—Oxide resistor furnace.

Among the limitations of resistance-type equipment is the melting point of the heating element and the supporting material. The lifetime of the heating element is also a limitation. In some instances heating elements can only be operated satisfactorily in atmospheres which are undesirable as far as the work piece is concerned. This means that an atmosphere barrier has to be placed between the heating element and the work. Those materials which can be used for the higher ranges of temperature are in many cases not available in a variety of shapes and sizes, so that problems of getting temperature uniformity are among the limitations. The versatility and the simplicity of this method are its major advantages and the reasons for its widespread use at all temperature ranges.

Induction heating is really one particular type of resistance heating. However, because of some basic differences it is generally classed separately. Figure 63–2 shows one type of induction heating equipment. High-temperature induction heating is attractive because (1) no electrical connections are required into the hot zone, (2) the primary coil can be operated at high-voltage—low current condition, and (3) one power supply can be readily adapted to many heating applications. Since this method also depends on the heating of a susceptor which

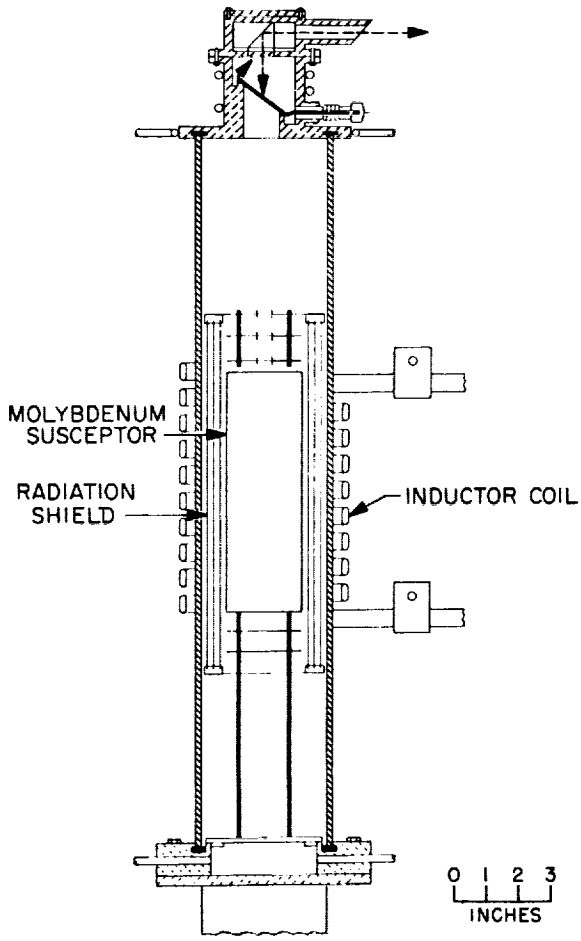

FIGURE 63–2.—Induction furnace.

then reradiates to the work, the limitations mentioned for the resistance heating also apply here.

Electric arcs were at one time the main source of high temperatures for laboratory techniques. But this method now finds its major use in the area of melting operations. Figure 63–3 is a simple schematic drawing of an arc melting unit. Obtaining temperature control and uniformity are two major problems which have limited the application of this method to areas such as melting. Recently, the arc heating method has received a major application in heating gas streams at high velocities. The so-called stabilized arc or plasma arc heating of gas streams to temperatures of 3000°C and above at supersonic velocities has been advanced to a high degree of utilization during the past few years.

In an attempt to overcome some of the limitations caused by the atmosphere in all of the previously mentioned heating methods, the imaging technique has been used for some applications. Figure 63–4 shows some imaging methods. In general, two sources have been used. One of these sources is the Sun, and the imaging method would be as shown in either (a) or (b) of Figure 63–4. The other widely used source is a carbon arc used with the imaging methods shown in (c), (d), and (e) of Figure 63–4. While the use of the Sun has the advantages of high temperature, ready availability, and long-time operation, it is limited by clouds, atmospheric absorption, and the need for solar tracking devices. In general, the main disadvantage of imaging equipment is that the heated area is small and concentrated, with rather severe thermal gradients. Techniques for reducing these gradients have been developed, but usually at the expense of temperature and total heat flux. For systems requiring atmospheric variation, the imaging technique has much to offer.

Electron bombardment is a recently developed technique for obtaining temperatures

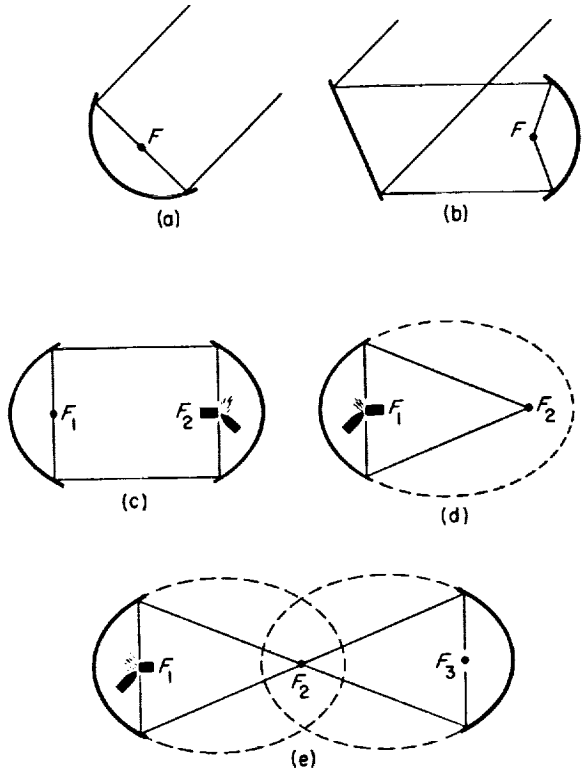

FIGURE 63–3.—Arc melting furnace.

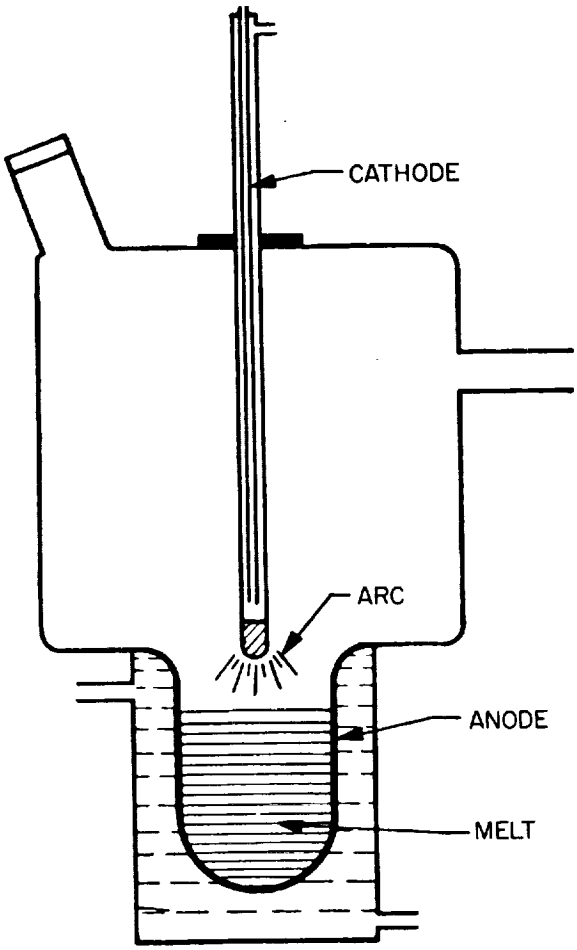

FIGURE 63–4.—Methods of imaging high-temperature sources.

above 1500°C. Figure 63–5 shows three applications of this method, the principle characteristics of which is that electrons emitted from a heated filament are accelerated toward an anode under high voltage. Under these conditions the main energy release is at the anode, which is heated. The major advantages of this method are that the currents required are in the range below one ampere and the electron beam can be restricted as to size and shape by various focusing methods. One major disadvantage is the fact that an evacuated chamber is required. However, this problem has now been partly overcome by the development of electron beam guns which can be separated from the work anode. Further improvements will no doubt be made in this method of heating which will make it a valuable laboratory technique.

LABORATORY USES OF HIGH TEMPERATURES

As indicated earlier, one of the major laboratory uses of steady-state high-temperature environments is the evaluation of materials as carried out in a testing program. Table 63–III lists some of the major laboratory uses in this specific area.

Design data and an understanding of the behavior of engineering structural material are best obtained from the various types of mechanical properties tests which have been standardized to a certain extent at approximately room temperature. It should be pointed out that extending these test procedures to temperatures above 1500°C can lead to difficulties which, in many cases, can be overcome only by compromise. It is perhaps in this particular area that workers in university laboratories

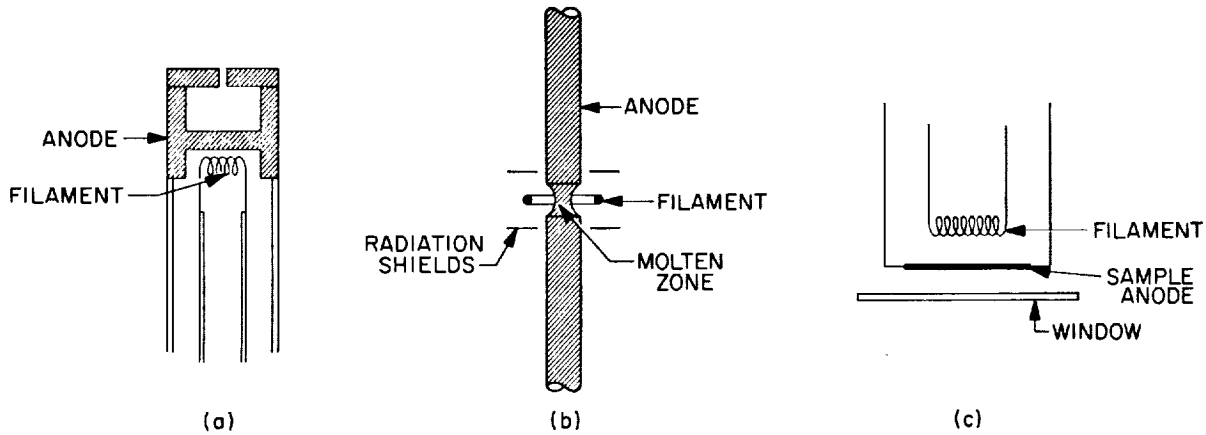

FIGURE 63–5.—Methods of using electron beam heating.

TABLE 63–III.—*Laboratory Uses of High Temperatures*

Evaluating mechanical properties of materials.	Tension. Compression. Torsion. Creep. Hardness.
Evaluating physical properties of materials.	Melting point. Vapor pressure. Phase equilibrium. Reactivity.
Special techniques	Microscopy. X-ray diffraction.

can make a much needed contribution. An evaluation of the effects of the various compromises on the high-temperature mechanical behavior of engineering structural materials is certainly an area where complete knowledge is lacking.

The university laboratories have been a major source of information in the area of material physical properties (see Table 63–III). One possible reason for this is that in many cases the information thus obtained is not of direct application to the engineering use of the material but is used mainly to understand and explain a particular behavior. The difficulties encountered in making these property determinations at temperatures above 1500°C are often greater than those indicated earlier. This is partly due to the fact that these properties are more sensitive to small variations in the material, and careful experimental techniques are therefore a necessity.

There is also an area of special laboratory techniques in which steady-state temperatures are used. The two techniques which are given in table 63–III are intended to serve only as an example and are not to be considered a complete listing. These techniques are also utilized largely in university laboratories. However, at the present time there is a very limited amount of work done above 1500°C and there is certainly a need for an expansion of this activity.

As indicated previously, a presentation of this type has to be general in nature and therefore cannot consider specific problem areas. It is hoped, however, that the need has been demonstrated for university laboratories to develop rather widespread use of steady-state temperatures above 1500°C so that the research necessary for our advancing technology can be carried out in the highly desirable academic surroundings. While there are problems to be solved in the development of such capabilities, a good start has been made toward the solutions.

64. High-Vacuum Techniques for Research

By Jack L. Taylor

JACK L. TAYLOR *is a Research Specialist in the Materials Research Section of Jet Propulsion Laboratory. He is conducting research on the mechanical properties of refractory metals at very high temperatures. Mr. Taylor was born in Montpelier, Idaho. He received his B.S. in Metallurgy from the University of California (Berkeley) in 1939, and his M.S. in Metallurgy from the Montana School of Mines in 1941. He is a member of AIME, ASM, Sigma Xi, and the American Vacuum Society.*

INTRODUCTION

The purpose of this paper is to discuss vacuum—what it is, how it is obtained, how it is used in research, and finally to conjecture about its future.

Man has already achieved a pressure so low as to be equivalent to one helium atom in a space sixteen times larger than our observable universe, that is, in a sphere whose radius is 10^{79} light years. This unusable vacuum was attained in a very small volume by the adiabatic demagnetization of a paramagnetic salt which was used to lower the temperature of helium vapor to 0.01°K. At this temperature, physicist Russell Scott (Ref. 1) estimates the vapor pressure of helium to be 0.3×10^{-316} torr [1] or about 10^{300} times lower than the vacuum of interplanetary space, estimated to be 10^{-16} torr.

The magnitude of these numbers is beyond comprehension. However, some concept of vacuum may be grasped by examining table 64–I (Ref. 2), in which pressure is described in terms of molecular density and mean free path. At the beginning of the high-vacuum region (10^{-3} torr), the mean free path of one molecule between collisions with other molecules is 5 cm, and there are 3×10^{13} molecules/cm^3. In the ultra-high region (10^{-12} torr) the mean free path is 5×10^{9} cm or 31,000 mi, and the molecular density is 30,000 molecules/cm^3.

Before discussing the techniques for reaching the low pressures of 10^{-3} to 10^{-12} torr, it is appropriate to ask why these techniques were developed. The vacuum-tube electronics industry furnished the first practical lure to the development of high-vacuum techniques. Fundamental and applied research in the chemistry and physics of solids gave further impetus to

[1] After Evangelista Torricelli; equivalent to 1 mm of Hg.

TABLE 64–I.—*Characteristics of Vacuum*

	Atmospheric pressure	Start of high-vacuum region	Intermediate vacuum	Ultra-high vacuum region		
Pressure (Torr)	760	10^{-3}	10^{-6}	10^{-8}	10^{-10}	10^{-12}
Mean Free Path of One Molecule between Collisions with other Molecules, cm.	6.5×10^{-6}	5	5×10^{2}	5×10^{5}	5×10^{7}	5×10^{9}
Number of Molecules per cm.^{3}	2×10^{19}	3×10^{13}	3×10^{10}	3×10^{8}	3×10^{6}	3×10^{4}

this technology. The first large vacuum chambers, other than those used for coating astronomical mirrors, were required by nuclear physicists. Finally, space exploration problems have heightened the interest in the production and use of high and ultra-high vacuums.

HIGH-VACUUM TECHNIQUES

The first problem confronting the vacuum technologist is to produce and maintain the desired order of vacuum. In every case, the vacuum attained represents a balance between the pumping capacity and the system gas-load. The gas-load results from gases adsorbed and absorbed on system walls and components, plus in-leakage through seals. An additional gas-load, significant in the ultra-high region, comes from the permeability of glass to helium and of metals to hydrogen. Successful solutions result when each gas source is minimized. Besides pumping, two other methods are often required to produce high vacuum, namely, baking to hasten outgassing, and trapping to prevent pump-fluid backstreaming.

Figure 64–1, a bar-graph, indicates the order of vacuum pressure achieved with various types of pumping. Pumping means which are novel or rarely used for research, such as catalytic

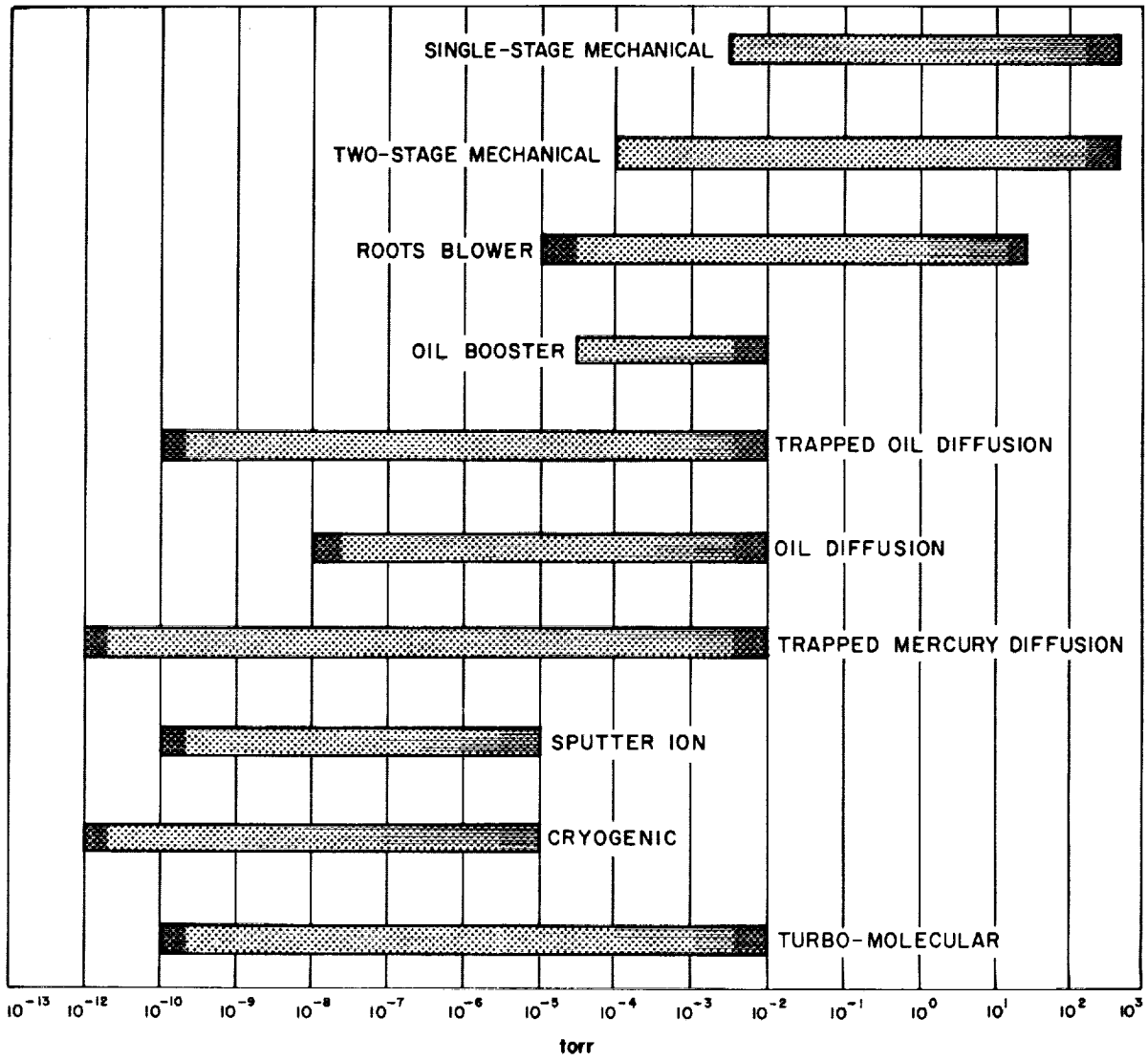

FIGURE 64–1.—Range chart for various types of vacuum pumping.

conversion, sorption pumping, and gettering, are not included. From this chart it is apparent that the high-vacuum region can be reached with a two-stage mechanical pump. This region can also be attained by a Roots blower backed by a mechanical pump, or an oil booster pump backed by a mechanical pump. To reach into the very high- and ultra-high-vacuum ranges, the diffusion pump is used, as are three more recently developed types of pump, namely sputter ion, cryogenic, and turbo-molecular drag pumps.

Diffusion Pump

In spite of the many different methods available to reach very low man-made pressures, the diffusion pump is the most widely used. Invented by Gaede in 1915, it used mercury as the pump fluid. The diffusion pump, usually with oil as the pump fluid, has continued to be improved in pumping speed and efficiency and is available in sizes ranging from less thain 1 in. to 48 in. in diameter. Liquid-nitrogen cold traps and molecular sieve traps have extended its capability into the ultra-high vacuum range. The ultimate vacuum attainable by a diffusion pump alone can never be better than the vapor pressure of the pump fluid above the pump inlet. In practice, effective trapping can suppress the back diffusion of pump fluid vapor so efficiently that the pressure is lowered by two orders of magnitude.

Mercury diffusion pumps are capable of producing a vacuum on the order of 10^{-12} torr, approvimately two orders of vacuum better than achieved with the best oil diffusion pumps. In addition, mercury in a diffusion pump is slightly more effective for hydrogen than any of the commonly used oils (Ref. 3). The vapor pressure of mercury at 90°K, attained with a liquid-nitrogen cold trap, is 3.5×10^{-29} torr (Ref. 4). With a well-trapped mercury diffusion pump, a system which is started clean stays clean, particularly if metal gasketing is used. Improvements in trap design, automatic equipment for controling the flow of liquid gases, and the availability of liquid gases have served to revive interest in large mercury diffusion pumps.

Ion Pump

Ion pumps are also used where a very clean vacuum is needed and where the processes carried out in the vacuum chamber do not produce large volumes of gas. The function of a sputter ion pump is illustrated schematically in Fig. 64–2. Electrons are emitted from the cathode plates and are accelerated toward the anode. The electrons are made to spiral by a magnetic field to enhance the probability of collision with gas molecules. Gas molecules struck by electrons are ionized and attracted to the negative collector plates where they are held by adsorption and in some cases react chemically with the material of the collector. The material of the collector plates is usually titanium. The bombardment of ions "sputters" the surface to provide fresh layers of metal with which chemically active gases combine.

It is apparent that the ion pump immobilizes gases within the system instead of removing them. Hence, its capacity is limited by saturation of the collecting surfaces. Another characteristic of the ion pump is that it removes chemically active gases faster than inert gases,

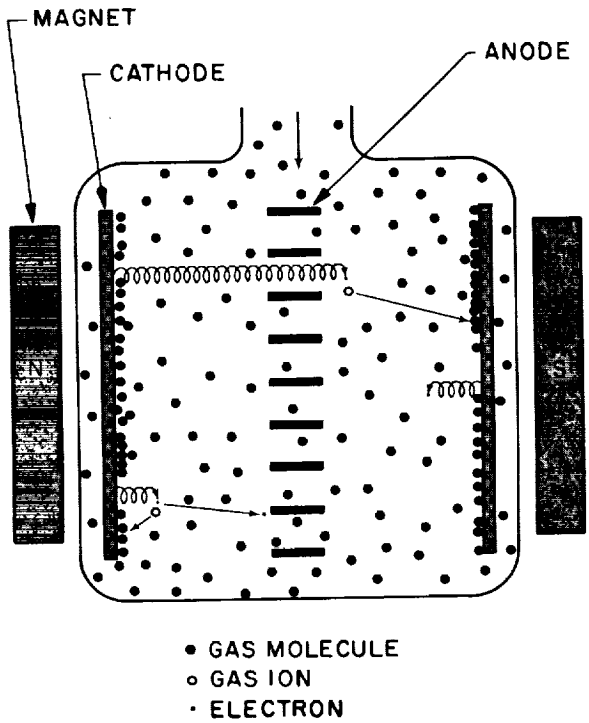

FIGURE 64–2.—Sputter ion pump (after Steinherz and Redhead).

because it pumps the active gases by both adsorption and chemical reaction. Furthermore, ion pumps re-emit a small fraction of the gases previously pumped because the ions reaching the collector surfaces dislodge some molecules which were already adsorbed. Ion pumping essentially ceases at 10^{-10} torr.

Cryogenic Pump

Cryogenic pumping can create a vacuum below 10^{-12} torr, even in large chambers. This process simply immobilizes gas by condensation on a very cold surfce. As shown in Fig. 64–3, a liquid gas (usually helium) is used to cool the condensing surface. Liquid-nitrogen cooled radiation barriers limit heat transfer from the experimental process in the chamber to the cold wall. The V-shaped baffle-form of the upper barrier allows molecules to pass. Cryogenic pumping requires back-up forms of pumping such as mechanical pumps, blowers, and diffusion pumps, which may or may not be valved off, depending on the experiment.

Cold-wall temperatures necessary to produce a vapor pressure of 10^{-7} torr for various gases to be pumped are shown in Table 64–II (Ref. 5). It is interesting that even a cold wall at 4° K, attainable with liquid helium, will reduce the vapor pressure of hydrogen to only 10^{-7} torr.

TABLE 64–II.—*Approximate Cold Wall Temperature Necessary to Attain a Vapor Pressure of 10^{-7} torr for Various Gases*

	Boiling point °K	Cold wall temperature °K
Hydrogen	20. 39	4
Neon	27. 3	8
Nitrogen	77. 34	24
Carbon Monoxide	81. 66	25
Oxygen	90. 19	27
Carbon Dioxide	194. 68 (sublimes)	82
Water	373. 2	175

The availability of cheap liquid gases has made cryogenic pumping practicable. This type of pumping may be advantageous for very large systems because the pumping speed is directly proportional to the area of the cold wall and is not affected by the conductance of connecting piping.

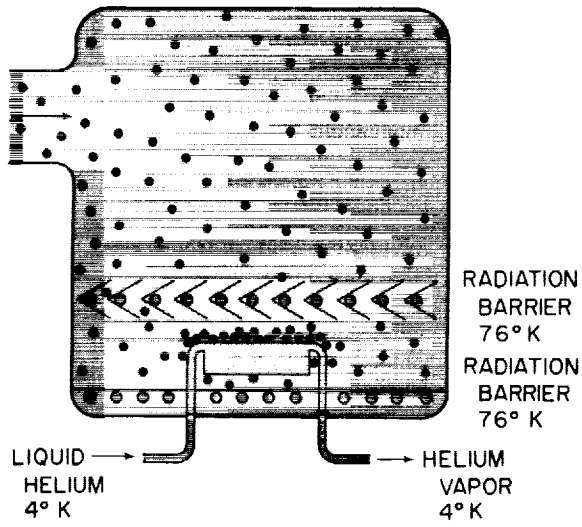

FIGURE 64–3.—Cryogenic pump (after Steinherz and Redhead).

Turbo-Molecular Drag Pump

The turbo-molecular drag pump (Fig. 64–4), a strictly mechanical device capable of producing a very clean vacuum on the order of 10^{-10} torr, has recently become available commercially in this country. It is based on the principle of providing a high probability of molecular flow in one direction by means of small clearances and proper rotor-stator relation. The pumping speed for air is virtually independent of pressure down to 10^{-10} torr. It has a good pumping speed for hydrogen to a pressure on the order of 10^{-6} torr. The development of this pump bears watching, although its usefulness may be limited because it is a high speed mechanical device and because of its (present) low capacity.

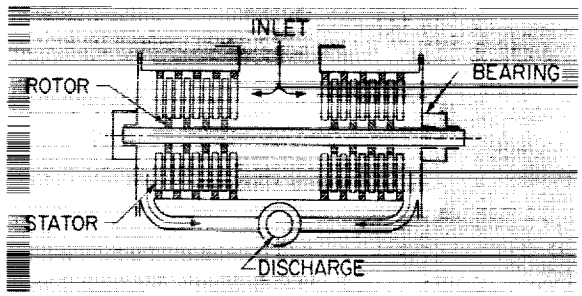

FIGURE 64–4.—Turbo-molecular drag pump.

Traps, Seals, and Baking

Liquid-nitrogen traps of various designs have been commercially available for some time. Another form of trapping, now commercially available, is the molecular sieve trap. It utilizes stable materials having very low vapor pressures, such as the artificial zeolites or activated alumina. These materials, which are produced in porous form with minute pore structures, are capable of trapping large quantities of gaseous impurities, although they do not readily absorb argon and hydrogen. They also provide a difficult path for surface migration through the trap. The trap can be reactivated by baking and pumping. The molecular sieve trap has become increasingly popular for use in the foreline piping to reduce backstreaming of mechanical pump oil into the vacuum chamber during preliminary evacuation or roughing.

Seal design and gasket materials have a major influence on the degree of vacuum reached and maintained. Thermal outgassing studies, coupled with mass spectrometry for gas species indentification, have led to the selection of elastomeric materials for seals which allow the ultra-high-vacuum region to be reached. One such material, Viton, a fluoro-elastomer has low permeability, low outgassing, and allows baking to 200° C.

The process of baking is often combined with trapped diffusion pumping to break the barrier between high and ultra-high vacuum when the process under investigation can withstand the application of heat. Effective sealing for bake-out in the range above 200° C., is accomplished with gold and aluminum wire between stainless steel flanges bolted together, with conical spring washers under the bolt heads.

Conductance

It is especially important for a vacuum system to have interconnecting plumbing, valves, baffles, and traps with sufficient conductance to match the speed of the pumping components. Conductance refers to the capacity of a tube, orifice, or component for carrying gas. The conductance, C, is the proportionality constant in the expression

$$C=\frac{Q}{(P_1-P_2)}$$

where Q is the quantity of gas flowing through the component, measured in units of pressure times units of volume/unit of time; and $P_1=P_2$ is the pressure drop across the component. The pressure unit in Q cancels the pressure unit in the denominator, leaving C expressed in units of volume/units of time (e.g., liters/sec).

The net conductance, C, of conductances C_1, C_2, C_3, etc., of components connected in series is

$$\frac{1}{C}=\frac{1}{C_1}+\frac{1}{C_2}+\frac{1}{C_3}+\ldots$$

If these same components are connected in parallel, the resultant conductance is

$$C=C_1+C_2+C_3+\ldots$$

In the high-vacuum region, the mean free paths of the molecules are so long that the molecules collide much more often with the piping walls than with each other. This condition of gas flow, called free molecular flow, can be assumed for practical purposes to exist when the pressure is such that the mean free path is half the diameter of the pipe or greater. In the free molecular flow region, conductance is independent of pressure and reaches its lowest value. It is dependent upon the molecular weight of the gas, the temperature of the gas, and the diameter and length of the pipe.

The net pumping speed, S', of the system is related to the speed of the pump, S, and conductance, C, by

$$\frac{1}{S'}=\frac{1}{S}+\frac{1}{C}$$

Thus, C must be considerably larger than S if S' is to remain a high percentage of S. A comprehensive treatment of vacuum system analysis is given in Refs. 4 and 6.

Gauging

The second problem confronting the vacuum technologist is the need to measure vacuum accurately. Until the Bayard and Alpert experiments of 1950, which led to improvement of the hot filament ion gauge, it was not possible to measure vacuum below 10^{-8} torr because of the X-ray effect suggested by Nottingham. In Fig. 64–5, a chart is shown indicating the range of pressures in which various gauges work. The

666582 O—62——26

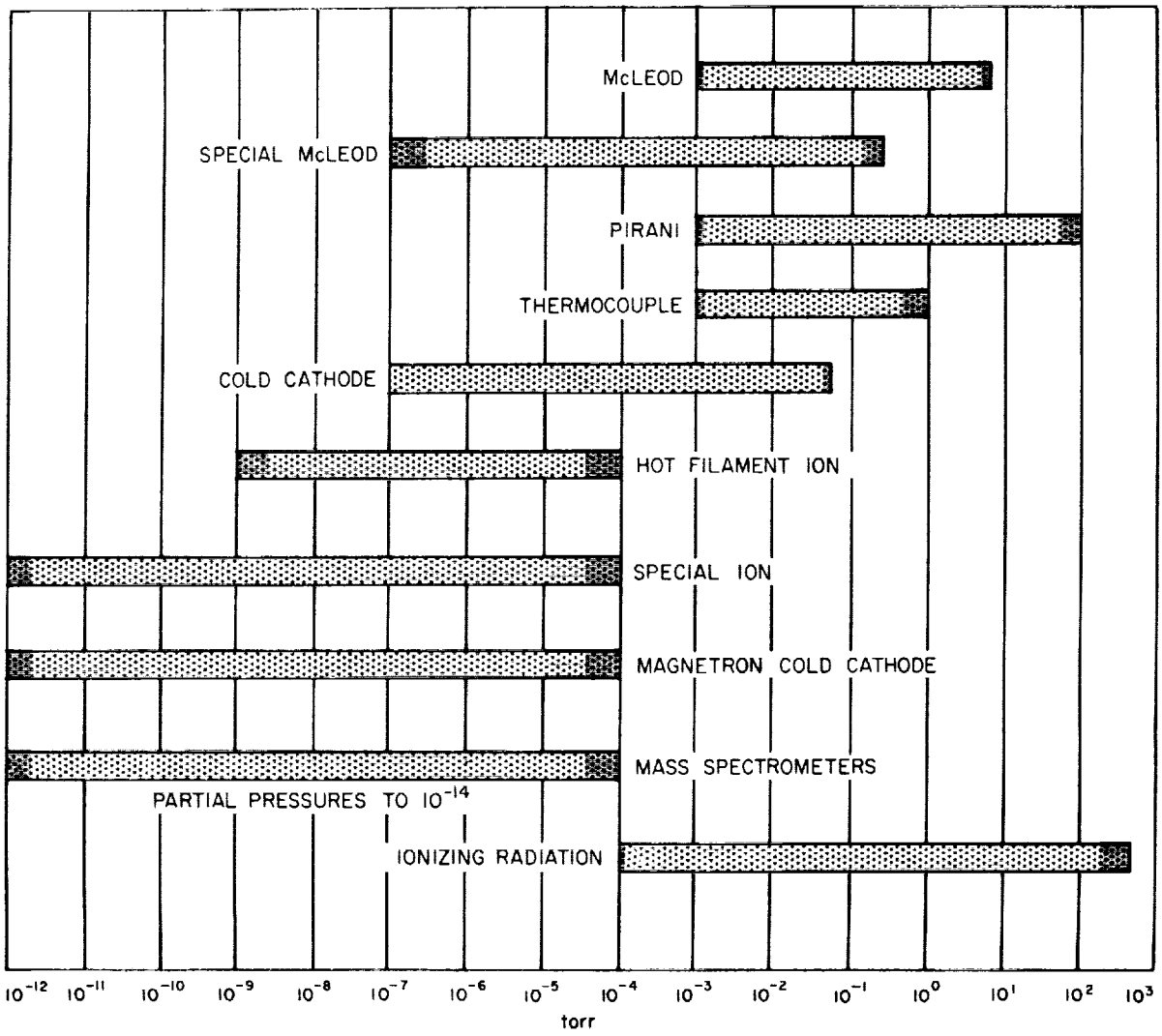

FIGURE 64-5.—Range chart for various types of vacuum gages.

improved cold cathode gauge is called the Magnetron, and the improved Bayard and Alpert hot filament ion gauge is designated the special ion gauge.

The hot filament ion gauge is the most widely used. Some of the factors which can cause errors at any pressure within its operating range are discussed by Redhead (Ref. 7). These factors are (a) pumping action of the gauge, (b) Barkhausen-Kurtz oscillations, (c) chemical effects at the hot filament and the bulb, and (d) variation of the residual current.

At 8 mA electron current and 250 v electron energy, the Bayard-Alpert gauge has a total pumping speed for nitrogen of 2 liters/sec when first operated. Chemical pumping accounts for 75% of the pumping speed, electron pumping the remainder. Tubulation with a conductance of 40 liters/sec must be used when the pumping speed of the gauge is 2 liters/sec, in order to keep the partial pressure of nitrogen in the gauge less than 5% of that in the chamber. For nitrogen, a 3-cm diameter, 5-cm long tube has a conductance of 40 liters/sec. The usual tubulation on the gauge has a conductance on the order of 2 liters/sec, which gives rise to an error of 100% in pressure measurement. Hence, the gauge pumping action can be offset by providing high conductance tubulation between the gauge and the chamber. The Barkhausen-

Kurtz oscillations, which cause sudden discontinuous pressure sensitivity at critical amplitudes, can be minimized by a transparent conducting coating (e.g., tin oxide) inside the bulb. The chief chemical effect at the hot filament is the dissociation of hydrogen, water, and hydrocarbons to give spurious ion currents. This effect can be reduced by pre-heating the filament in 10^{-7} torr of oxygen at 2000°K to lower the carbon impurity content, and by using low work-function coatings to lower the operating temperature of the filament. At very low pressures, the residual current due to X-ray effects and ultraviolet radiation from the filament is of the same magnitude as the ion current. One method of determining the residual current involves adding a modulator electrode to the usual Bayard-Alpert gauge design. A modulator factor is determined by measurements at high pressure where the residual current is negligible. With this information, the true ion current can be found by a difference method.

From the discussion above, it is obvious that a single ion gauge design will not have constant sensitivity across the pressure range from 10^{-5} to 10^{-12} torr. Furthermore, total pressure measurements below 10^{-9} torr lose significance when differential pumping action takes place in the gauge; partial pressure measurements are preferable. Partial pressure measurements in the ultra-high-vacuum range are made with specialized mass spectrometers, such as the Omegatron, which identify the gas species. A recently developed modification of a 90-deg sector mass spectrometer by Davis and Vanderslice of the General Electric Company can measure partial pressures a low as 10^{-14} torr. New developments in gauge design promise measurements down to 10^{-18} torr.

APPLICATION OF TECHNIQUES

Several examples have been prepared to illustrate how vacuum, once achieved and measured, is put to use in research.

High-Temperature Tensile Furnace

In the tensile furnace illustrated in Fig. 64–6, vacuum provides a protective atmosphere. The furnace is used to measure the deformation behavior of refractory metals in tension at temperatures up to 2980° C. A vacuum atmosphere is required because of the high reactivity of the refractory metals with air gases at temperatures as low as 500° C. The elements, oxygen, nitrogen, carbon, and hydrogen, which dissolve interstitially, influence markedly the mechanical properties of the refractory metals at low and intermediate temperatures even when present in a few parts per million. The degree of vacuum can change the impurity level during testing, depending upon the temperature and the particular metal being tested. For commercially pure tungsten, having total interstitial element impurity levels of 50 ppm or less, a vacuum of 10^{-5} torr and a temperature of 2900° C maintained for 10 min appear to leave the composition relatively unchanged.

The furnace has a hot zone 2½ in. in diameter by 8 in. long provided by a heater assembly consisting of a thick-walled tungsten susceptor surrounded by very thin, split, tungsten radiation-shields. The assembly is supported within an induction coil by tungsten rods resting on an insulating zirconia cylinder. Power is supplied by a 50-kw, 10,000-cycle motor generator set. The grips and specimen are entirely surrounded by the hot zone, insuring a uniform temperature in the specimen.

The vacuum in the 10^{-5} torr range is provided by two baffled and cold-trapped 4-in. diffusion pumps backed by an 80-cfm mechanical pump. A 7-cfm holding pump in conjunction with high-vacuum valves above the diffusion pumps adds convenience and flexibility to the system. After conductance losses in trapping and piping, the two diffusion pumps have pumping speeds of between 400 and 500 liters/sec at the furnace port. The conductance of the furnace port is 430 liters/sec. The full capacity of the pumping system is required to maintain 10^{-5} torr against the outgassing load at the higher heating rates. Typically, a tensile test at 2980° C takes 2½ hr to reach temperature, 10 min holding time, and 20 to 30 sec testing time at a strain rate of 2.0 in./in./min.

Cryogenic Gyro

The cryogenic gyro is a device which may provide inertial guidance systems for spacecraft.

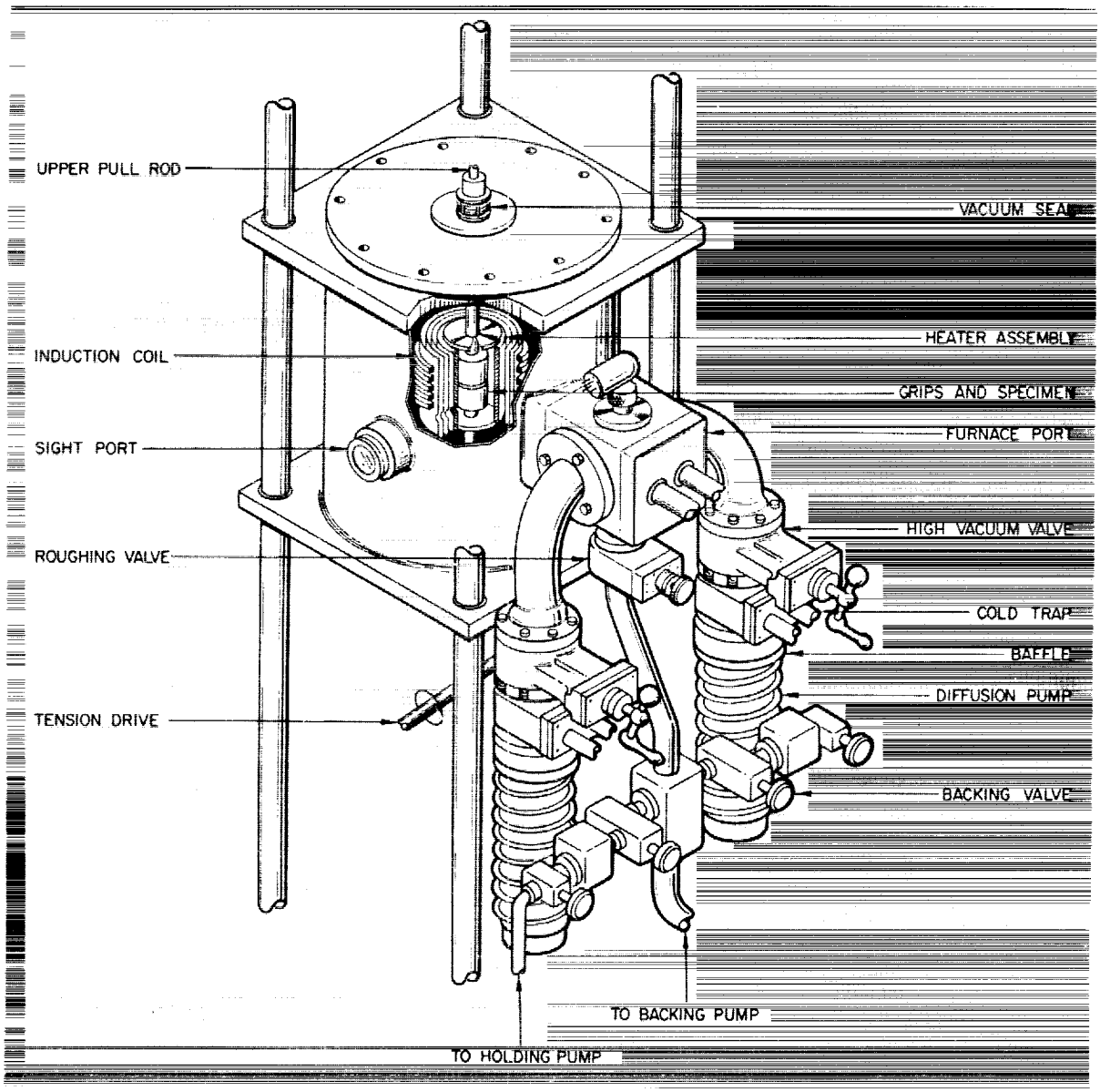

FIGURE 64-6.—High-temperature tensile furnace.

It depends on vacuum and extremely low temperature for its operation and is made possible by the fact that the magnetic forces on a superconductor are normal to its surface.

FIGURE 64–7.—Photograph of cryogenic gyro.

Figure 64–7 shows a photograph of the gyro (Ref. 8), with a ½-in. niobium sphere levitated in a liquid helium bath. The gyro is shown schematically in Fig. 64–8. The starting coils are used to induce a current to flow in the "normal" coils in the direction indicated by the arrows. This current is then trapped in the coils by introducing liquid helium, which quickly cools the coils and rotor to superconducting temperature. The trapped current provides a magnetic field whose forces are normal to the superconducting rotor, causing levitation. After superconducting temperature is attained, the helium is pumped away. At the same time, a small jet of helium gas sets the levitated rotor in rotation, and the multiwalled Dewar operates to maintain the superconducting temperature. The rotor should continue to rotate on its magnetic suspension indefinitely, if the superconducting temperature is maintained.

Pumping proceeds until a vacuum on the order of 10^{-7} torr is reached in the chamber. This order of vacuum is a compromise requirement. The vacuum must be such that there are enough molecules to transfer heat by conductance from the cold walls to the coils and sphere to keep them superconducting, yet not so many molecules as to slow the rotation of the sphere by molecular drag. Pumping of the chamber and the Dewar chambers is done with a 4-in. diffusion pump, backed by another 4-in. diffusion pump, in turn backed by a small mechanical forepump. It is thought that this series arrangement gives better helium pumping by providing a lower pressure drop across the first diffusion pump.

Bacteria Survival

An exceptional use of ultrahigh vacuum is made in a biological experiment to determine the ability of microorganisms to withstand space environment. A study of bacillus subtilis, variety niger, required that a vacuum of 10^{-8} torr or better be maintained for a period of at least 30 days (Ref. 9). It was necessary that the vacuum chamber be completely clean and sterile before introduction of the microorganisms, and during the period of vacuum exposure contamination had to be held to a minimum. No pump fluid gases could be allowed in the chamber. Furthermore, the vacuum had to be achieved without bake-out which might injure the microorganisms.

The apparatus used for the experiment is shown schematically in Fig. 64–9. The microorganisms were placed in the test tubes in the vacuum chamber, and a vacuum was pumped with a three-stage mercury diffusion-pump backed by a small mechanical forepump. Backstreaming of mercury vapor was controlled by a liquid-nitrogen cold finger placed over the top jet of the diffusion pump and by a separate liquid-nitrogen cold trap. A final barrier against back diffusion of mercury was provided by a gold film evaporated on the elbow connection to the chamber. Any mercury molecules travelling this far would hit the elbow wall and be immobilized by amalgamation with the gold.

Outgassing from the glassware in the ultrahigh-vacuum region was minimized by careful

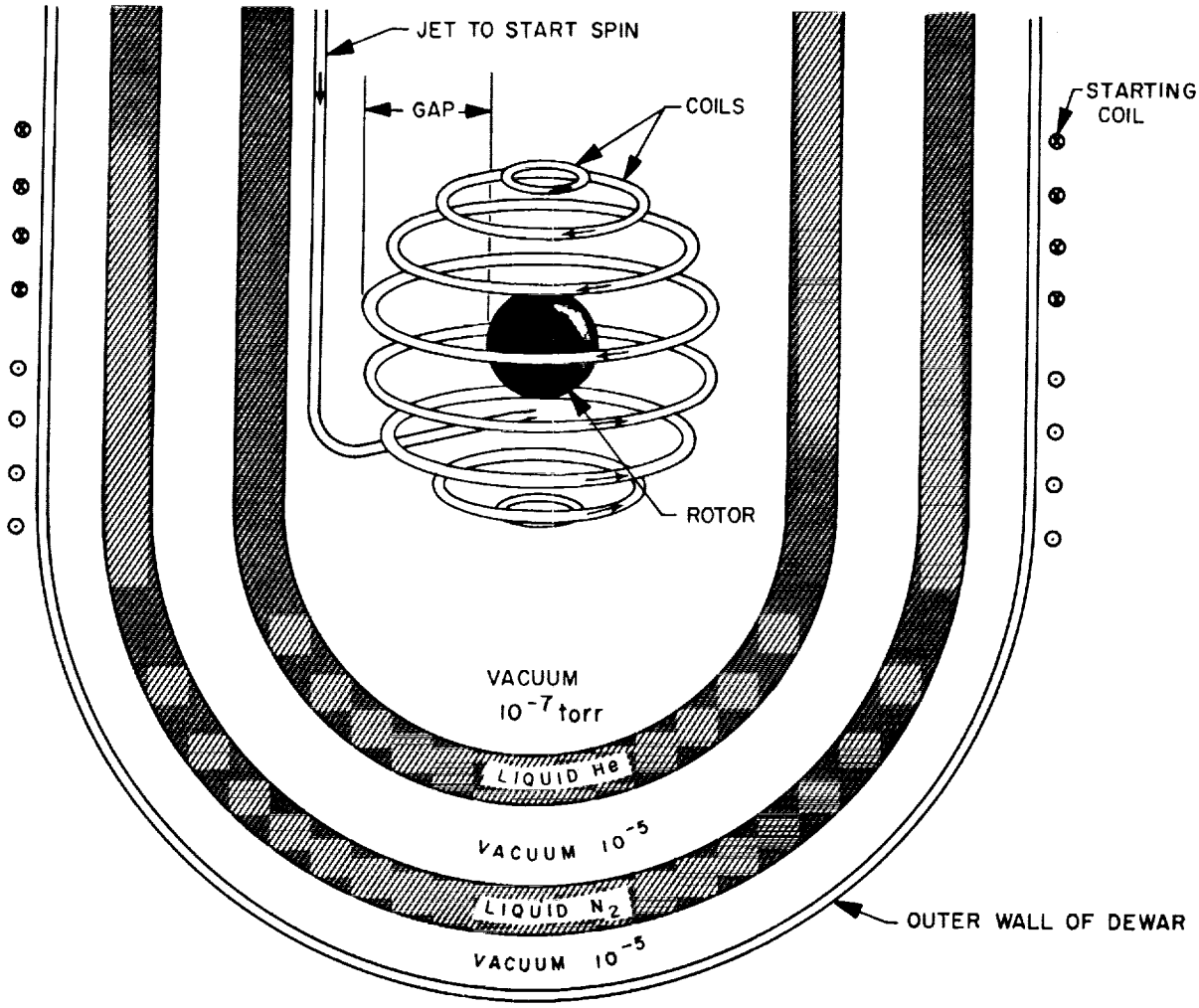

FIGURE 64–8.—Cryogenic gyro.

cleaning before assembly. Seven steps of degreasing, washing with bases, washing with acid, and alternate rinsings were performed.

The system functioned, as designed, between 3×10^{-8} and 6×10^{-9} torr for a period of 35 days. A Bayard-Alpert type hot filament ionization gauge remained in continuous operation throughout the experiment. The experiment showed that bacillus subtilis, variety niger, will survive an ultra-high vacuum of 10^{-8} torr for a period of 35 days.

FRICTION AND WEAR

A complicated ultra-high-vacuum system is that used in the friction and wear apparatus shown in Fig. 64–10. Buckley and Johnson (Ref. 10) are using the apparatus to measure the lubrication properties of gallium-rich films in a vacuum of 10^{-10} torr. This is a surface physics problem which sets stringent requirements upon the degree and cleanliness of the vacuum. At 10^{-6} torr, it is known (Ref. 11) that a clean metal surface is contaminated by a monolayer of gas in a few seconds. At 10^{-9} torr, it is estimated that a monolayer forms in approximately 17 min.

To achieve desired conditions, the procedure is the following: The entire apparatus is covered with a bake-out oven and hood while being pumped with a vane-type pump backed with an oil-sealed rotary pump of 13-cfm capacity. A liquid-nitrogen cold trap and a molecular sieve trap are placed in series in the piping between the vane-type pump and the vacuum

chamber. The two mechanical pumps first mentioned continuously pump the forechamber, which contains the driven part of the magnetic drive, to preclude contamination of the main chamber with bearing lubricant. These pumps are valved off the main chamber when it reaches 10^{-4} torr, and a 400-liter/sec ion pump is started. Baking proceeds during ion pumping, until the chamber reaches the 10^{-8}-torr range. The hood and bake-out oven are removed, and an electron-beam heater is focussed on the disk and rider specimen area to further degas that area. The electron-beam heat source is also used to maintain temperatures to 1000°F during the friction experiment.

Although ion pumping is continued, the final pressure in the low 10^{-10} torr range is achieved when the cold trap at the top of the chamber is filled with liquid helium. Occasionally, dry nitrogen purging and repumping is used after the oven bake-out.

For the friction measurements the rider specimen is loaded by the lever and weight principle with the gimbal assembly acting as the fulcrum. The disk specimen, rotated by the magnetic drive, rubs against the rider specimen, applying a torque to its holder shaft. The friction is proportional to the torque, which is measured with strain gauges. A photo-

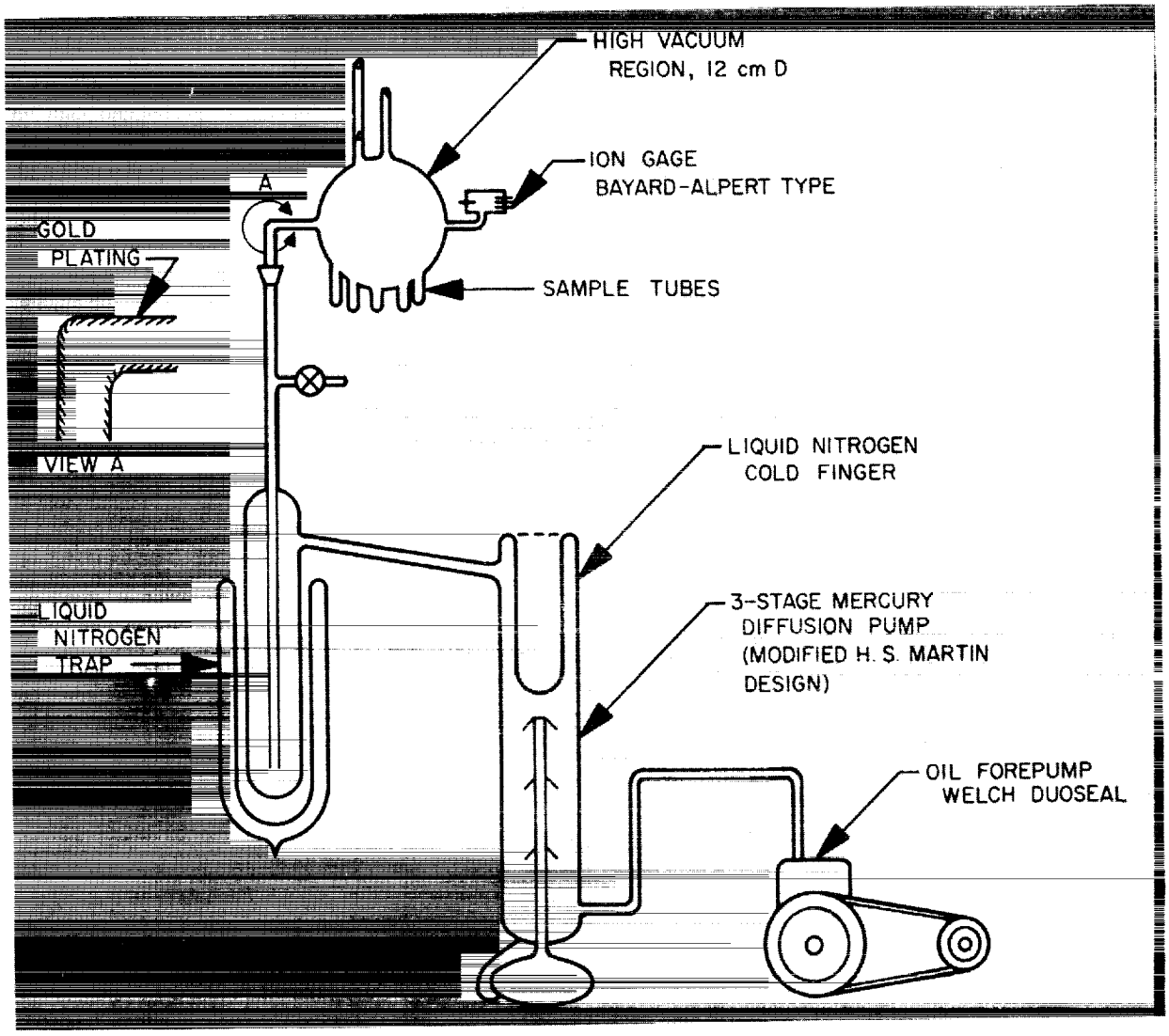

FIGURE 64-9.—Vacuum environment apparatus for bacteria survival test.

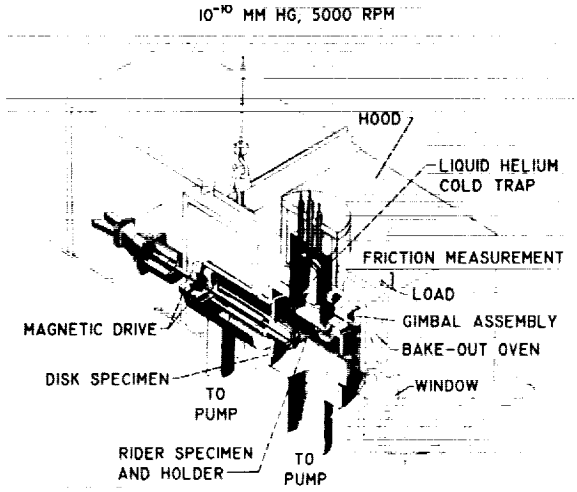

FIGURE 64–10.—Friction-and-wear apparatus (Buckley and Johnson, NASA Lewis).

graph of the equipment, viewed from the magnetic-drive end, is shown in Fig. 64–11.

This ingenious experimental apparatus combines two types of mechanical pumping, foreline trapping, and ion and cryogenic pumping with oven bake-out and electron-beam heating to meet the vacuum requirements.

Ion Propulsion Engine

The ion propulsion engine (Ref. 12) is designed for long-duration missions in space and will only operate in a vacuum. It depends for its thrust upon ions accelerated away from the spacecraft. The amount of thrust is proportional to the mass flow rate and the velocity of the ions.

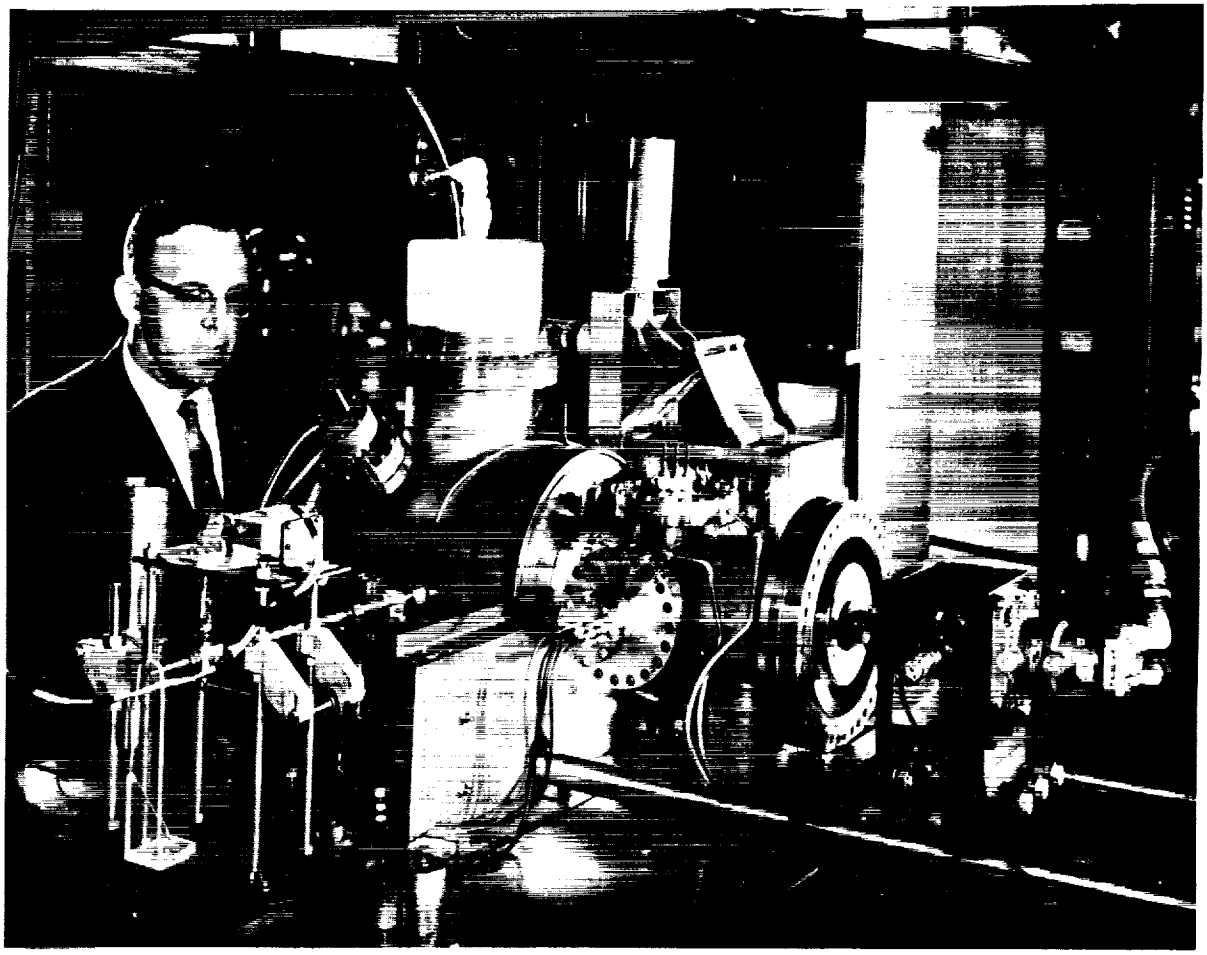

FIGURE 64–11.—Photograph of friction-and-wear equipment.

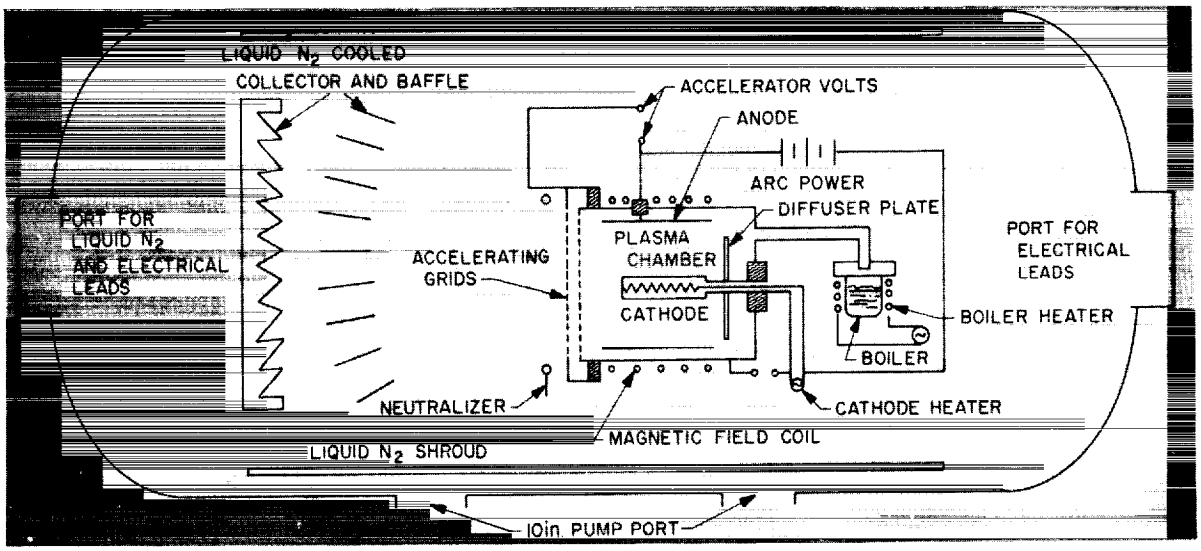

FIGURE 64–12.—Ion propulsion engine and chamber.

The engine is illustrated schematically in Fig. 64–12. The metal used for engine fuel, usually mercury or cesium, is vaporized in the boiler and diffused into the plasma chamber. Electrons are accelerated from the hot cathode toward the anode by means of a potential difference and are forced to take cyclotron orbits a few millimeters in diameter in the magnetic field introduced by the magnetic field coil. This path enhances the probability of the electrons colliding with the metal vapor atoms to produce ions before the electrons reach the anode. Ions migrating in the field gradient which reach the accelerating grids are accelerated away from the engine by the high potential between the grids. Surplus electrons from the ionizing process, upon reaching the anode, are pumped to the neutralizer and allowed to leak out, emerging with the ion beam. The neutralizer insures that the spacecraft will not become increasingly negatively charged and the engine cease to function. A photograph of the ion engine on its mount is shown in Fig. 64–13.

The optimum vacuum range for an efficient production of metal ions in the plasma chamber seems to lie between 10^{-3} and 10^{-4} torr. In the external environment, a higher vacuum, at least 10^{-6} torr, is necessary to allow the ions

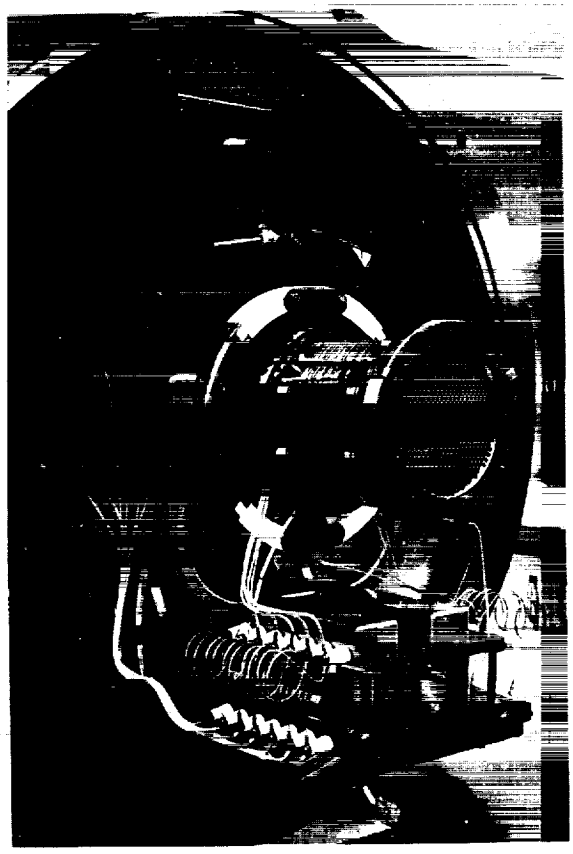

FIGURE 64–13.—Photograph of ion propulsion engine on its mount.

to escape from the engine without excessive collisions between the residual gas and the directed ion beam (which would cause ion deflection and charge exchange). Furthermore, the condition of space which allows the ions to stay away and not return to the engine or bounce back into the beam must be simulated in laboratory testing.

These vacuum requirements are met by placing a liquid-nitrogen baffle and collector in front of the ion beam, as shown in the schematic of Fig. 64–12. The condensing surfaces of the baffle and collector are arranged in an optical trapping configuration. Stray metal atoms which escape the baffle and collector are immobilized on a liquid-nitrogen cold shroud. In practice, the vacuum facility is taken initially into the 10^{-6} torr range using two 10-in. liquid-nitrogen-trapped diffusion pumps. With the engine in operation at a fuel flow rate of 5 grams of mercury/hr, the baffle, trap, and shroud must pump mercury vapor at the rate of 100,000 liters/sec to maintain the initial pressure. In fact, the cryogenic pumping, with a surface area of about 30 ft^2, is so effective that the chamber pressure continues to drop even with the engine operating and the diffusion pumps valved off.

A photograph of the over-all installation is shown in Fig. 64–14. Measurements of the engine's thrust are made on a thrust mount having a sensitivity of 2 μ lb. The vacuum tank is bolted to a 28,000-lb block to insure that resonance frequencies are too low to interfere with the measurements. Two 130-cfm mechanical pumps which back the diffusion pumps are mounted 50 ft away, with the connecting piping vibration damped.

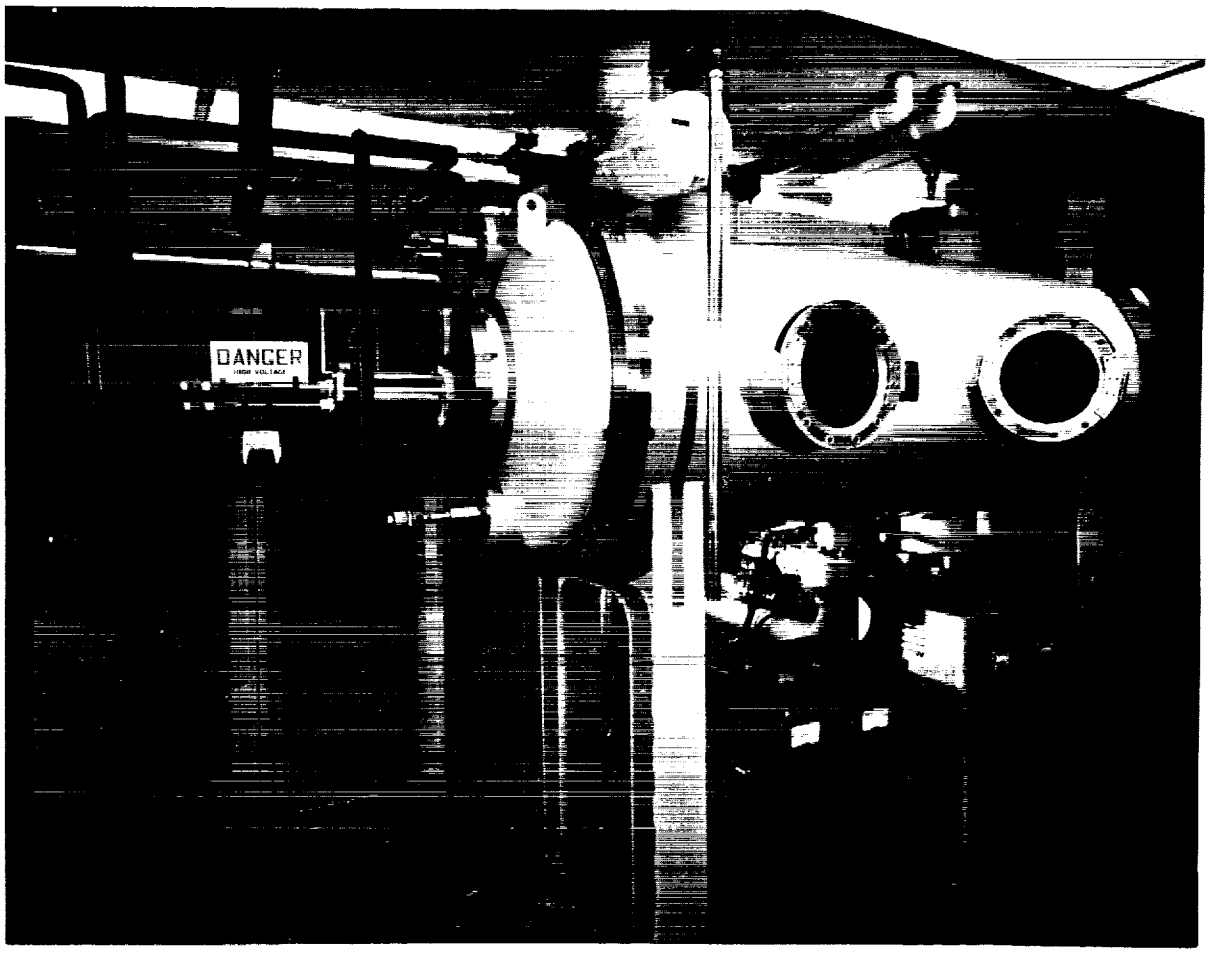

FIGURE 64–14.—Photograph of installation for testing ion engine.

Fission Electric Cell

In a discussion of ion propulsion, it is natural to ask what source might be used to provide the high-voltage, low-current power the engine needs during space flight. One possibility is the fission electric cell (Ref. 13) shown in Fig. 64–15. The cell converts nuclear energy directly to electrical energy in the following way: fragments from fissionable material coating the cathode traverse the vacuum space to the anode with energy levels of about 80 Mev and a net charge of +20 e. A potential of 4,000,000 v between the cathode and anode is theoretically possible. However, knock-on and follow-out electrons emerge with the fission fragments and interfere with the available electrical energy. An electromagnet is used to repress the electrons and realize a useful voltage across the cell. Vacuum environment allows the fission fragments to carry energy without wasting it by colliding with an ionizing gas molecules. It also prevents high voltage breakdown in the presence of the ionizing source.

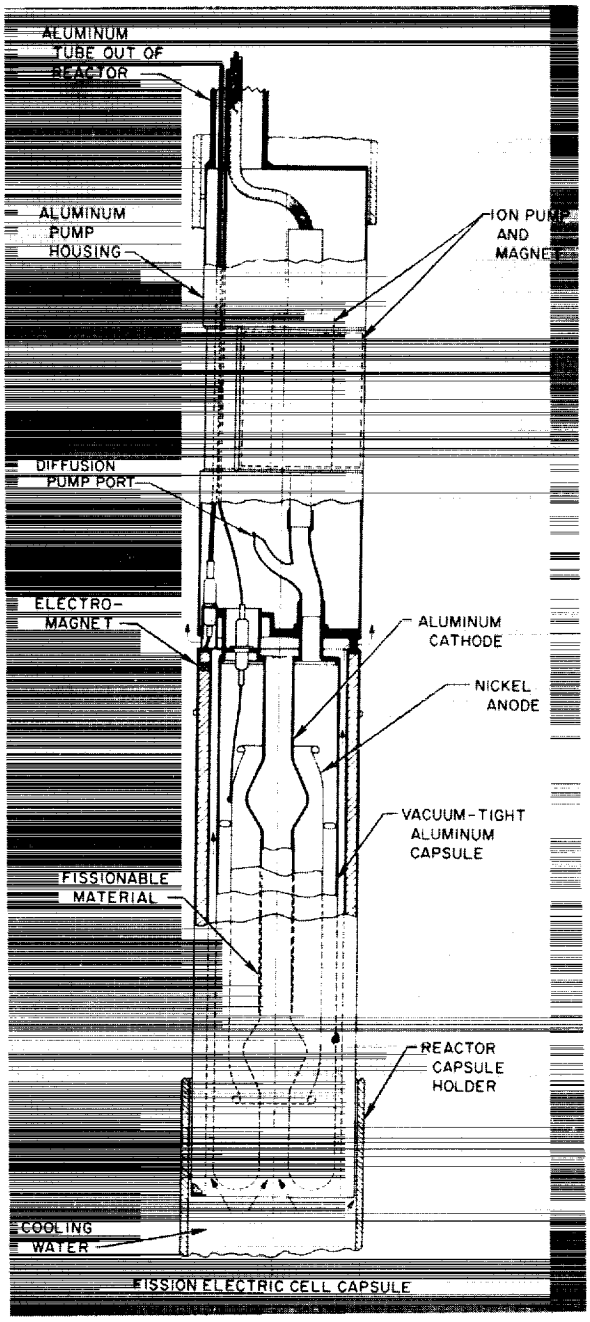

FIGURE 64–15.—Fission electric cell.

The experimental cell, an all-welded aluminum construction 3 in. in diameter, is tested in a neutron flux 25 ft under water. Since the cell is out of reach during operation, dynamically pumping it to maintain a satisfactory vacuum presents a problem. The initial vacuum in the cell is achieved by diffusion pumping and bake-out, limited to 100° C by the aluminum construction. After pumping to approximately 10^{-6} torr, the diffusion-pump port to the cell is pinched off, and the cell is placed in the reactor. The vacuum is maintained with a 1 liter/sec ion pump incorporated in the cell. The gases to be pumped are principally xenon and krypton, the fission fragments, which limit the efficiency of the cell when the pressure is too high. Gamma radiation plus Compton-effect electrons ionize the adsorbed and absorbed gases not previously removed by the bake-out, thereby adding to the gas load on the ion pump.

Space Simulator

The Jet Propulsion Laboratory space simulator (Ref. 14) which has a vacuum chamber 25 ft in diameter by 25 ft high, is an example of the application of vacuum technique applied on a very large scale. A photograph of the simulator with the door open and the spacecraft Mariner in view is shown in Fig. 64–16. The simulator is designed to test spacecraft under simulated interplanetary conditions of intense solar radiation, radiation heat sink, and high vacuum. The vacuum is achieved by cold-trapped diffusion pumping. The radiation heat

sink of outer space is simulated by a liquid-nitrogen cold shroud with a coated surface having an emissivity of at least 0.9 for both ultraviolet and infrared radiation. The solar radiation is simulated by an array of 131 mercury-xenon arc lamps, which produce a design solar flux intensity of 200 w/ft^2.

Figure 64–17 shows the solar-simulator optics. The light from the mercury-xenon arc lamp source array is reflected from flat circular mirrors arranged as facets on a parabola to a pseudo-hyperbolic reflector, thence through a quartz lens into the chamber. The virtual source, consisting of multifaceted pebbles, reflects light to spherical mirrors which, arranged as facets on a parabola, provide the even distribution of solar radiation. The primary virtual source casts a shadow into the working volume. This is filled in by a lens in the primary virtual source, an auxiliary pebble bed, and a parabolic reflector. The optical system has a collimation requirement of ± 5 deg for the extreme ray. The mercury-xenon arc lamp, which does not match the solar spectral distribution curve as well as a carbon arc lamp, has less fluctuation and can be controlled more closely. A further departure from the solar spectral distribution is caused by the aluminum reflecting surfaces. However, meaningful tests can be conducted by correcting the observed spacecraft temperature for spectral reflectance and absorbency.

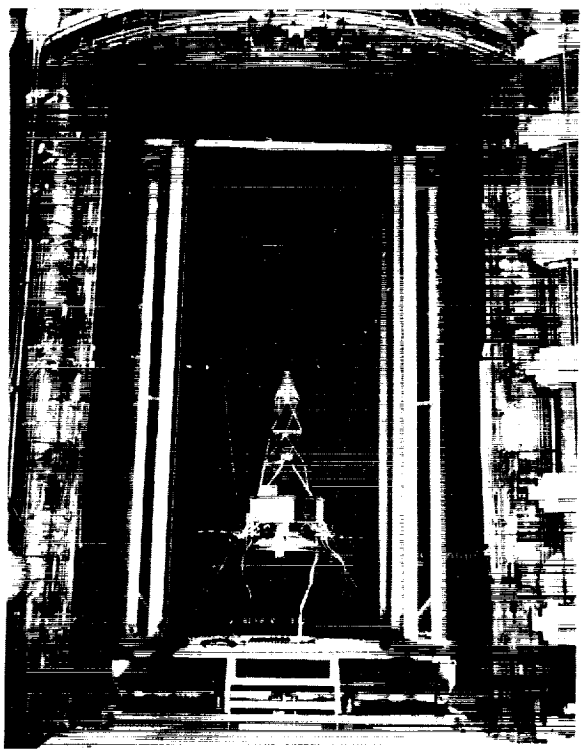

FIGURE 64–16.—Photograph of space simulator.

A vacuum on the order of 10^{-4} torr is sufficient to insure that heat transfer by radiation is 99% of the total heat transfer, conductance accounting for less than 1%. However, the design pressure for the clean, empty, outgassed chamber is 5×10^{-6} torr, which allows some margin for the unknown gas load of future spacecraft under solar heat flux. The pumping schematic for the chamber is shown in Fig. 64–18. Compressors in a nearby wind tunnel are used to rough the chamber to less than 2×10^{-4} torr, after which two 5000-cfm blowers (Stokes 1713), backed by a combination 1200-cfm blower and 300-cfm mechanical pump (Stokes 1711), further reduce the chamber pressure to 10^{-2} torr. At this pressure, ten 36-in. oil diffusion pumps, which are held by a 130-cfm pump (KDH 130) during roughing, are valved in to reduce the chamber to the desired operating pressure. The diffusion pumps are liquid-nitrogen trapped to preclude contamination of the optics with pump oil films, which would gradually reduce the light intensity. When the system is at operating pressure, the shroud is filled with liquid nitrogen. Approximately 5000 gal are required to bring the piping and shroud system down to liquid nitrogen temperature. The 9500 ft^2 of shroud, in addition to simulating the radiation heat sink of outer space, also provide extra pumping capacity to handle outgassing from the spacecraft.

A vacuum system of this size is a major achievement, considering the myriad of weld joints, braze joints, and seals which must be leak-free, the thermal expansion in the liquid-nitrogen shroud and plumbing, and the huge-size pumping and its control. When the large complex optical system is considered as an integral part of the vacuum chamber, the achievement is even greater.

The examples discussed here are but a few of the many ways in which research projects utilize vacuum. Some examples of research highly

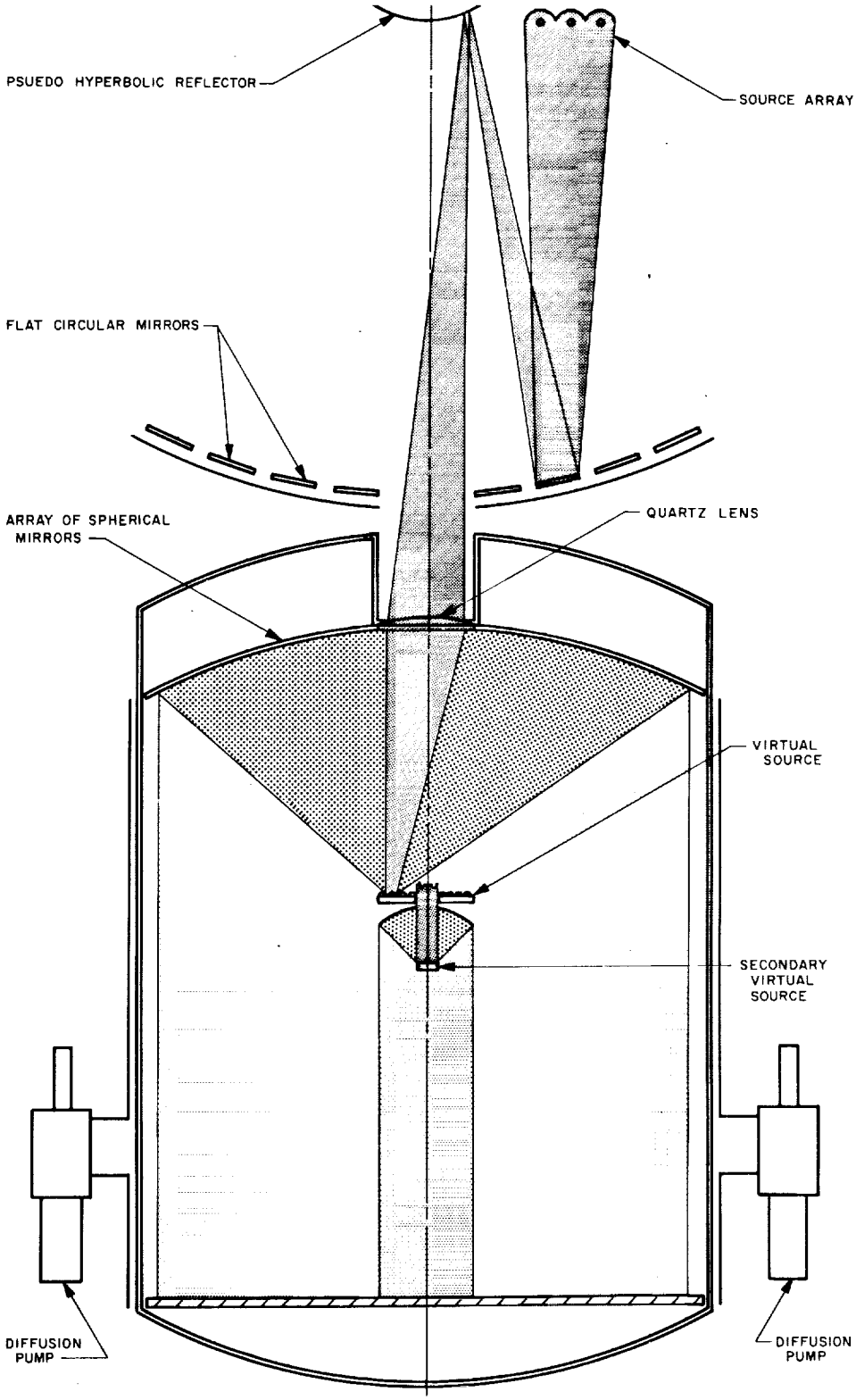

FIGURE 64–17.—Solar simulator optical arrangement.

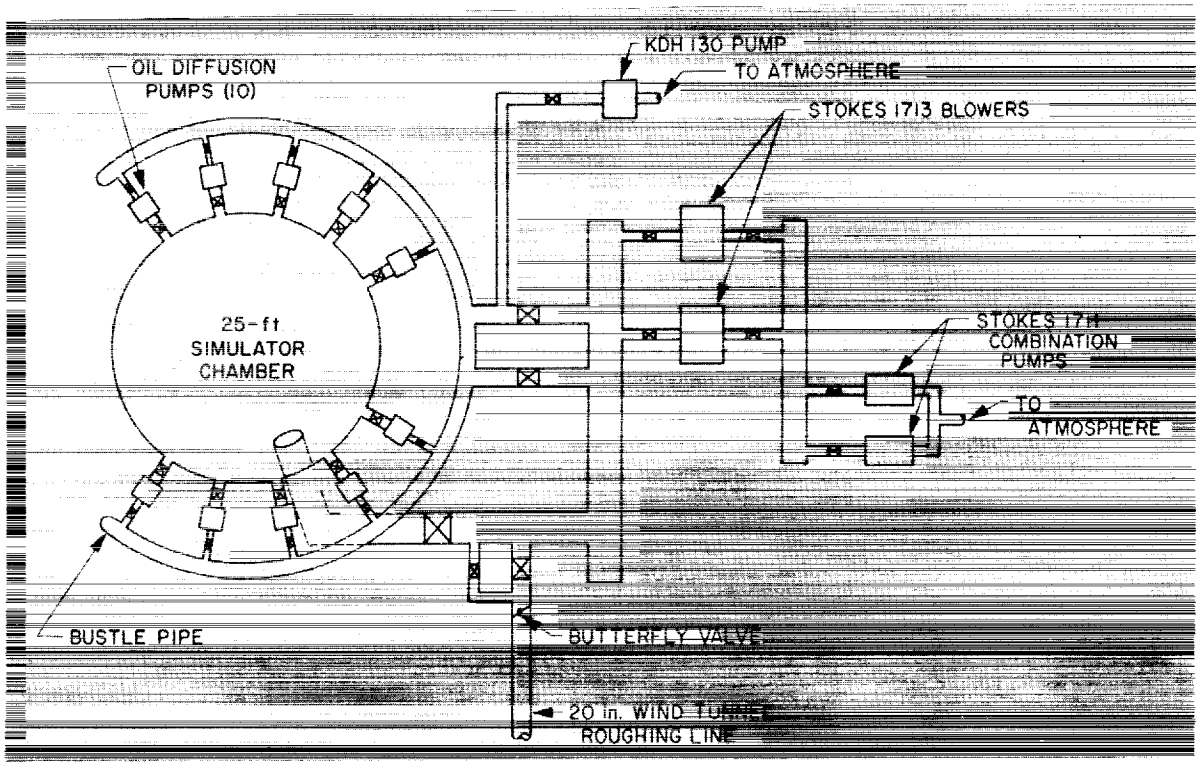

FIGURE 64–18.—Vacuum pumping schematic for solar simulator.

dependent of vacuum technology are investigations of vacuum deposition of thin films for optical, semiconducting and superconducting purposes; the degradation of polymers; zone refining of metals; and instrumentation for space exploration, such as gas chromatography and ultraviolet spectrometry.

FUTURE OF VACUUM

What is the future of vacuum technology? For those who would build large ultra-high-vacuum systems, Balwanz (Ref. 5) has made an estimate of the relative operating costs of pumping by cryogenic means and by diffusion pump methods. In Fig. 64–19, three types of cryogenic pumping are shown. These are a one-stage pump consisting simply of a liquid-helium cold wall, a two-stage pump with liquid-

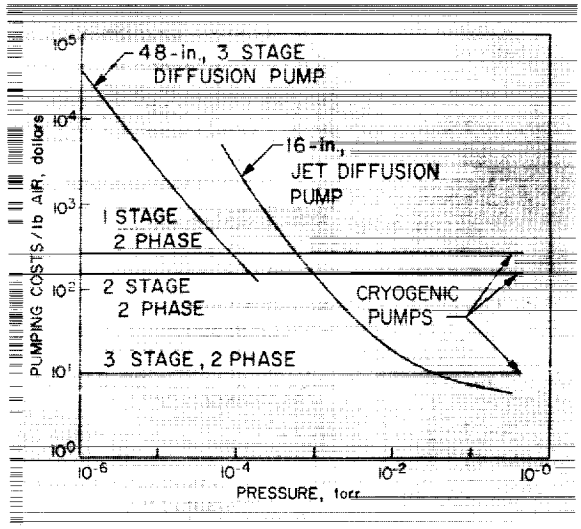

FIGURE 64–19.—Comparative operating costs of cryogenic and diffusion pumping.

helium and liquid-nitrogen cold walls, and a three-stage pump, the most complicated and efficient form of cryogenic pump, involving a liquid-helium cold wall, guarded by a liquid-hydrogen radiation baffle, which in turn is guarded by a liquid-nitrogen radiation baffle. The comparison indicates that cryogenic pumping, even in its simplest form, is cheaper than diffusion pumping for very large systems.

One nationally known vacuum equipment manufacturer claims in a news bulletin (Ref. 15) of August 1962 to have created a vacuum of 10^{-15} torr in a volume of approximately 6 ft^3. This pressure is at the limit of sensitivity of the best gauges and even the best mass spectrometers. The capability for achieving vacuum appears to have surpassed again the capability for measuring it. The degree of vacuum already produced will serve a great percentage of research needs. However, man will continue seeking higher and higher vacuum and the methods for measuring it.

REFERENCES

1. Scott, Russell B., *Cryogenic Engineering*, D. Van Norstrand Co., Inc., Princeton, New Jersey, 1959.
2. Steinherz, H. A., and P. A. Redhead, "Ultrahigh Vacuum," *Scientific American*, Vol. 206, No. 3, 1962, pp. 78–90.
3. Yarwood, J., *Symposium on Some Aspects of Vacuum Science and Technology, London, January, 1962.* British Journal of Applied Physics, Vol. 13, No. 7, 1962, p. 304.
4. Dushman, Saul, *Scientific Foundation of Vacuum Techniques*, John Wiley and Sons, Inc., New York, 1949, p. 782.
5. Balwanz, W. W., J. R. Singer, and N. P. Frandsen, *High Pumping Rate Vacuum Systems*, Seventh National Symposium on Vacuum Technology Transactions, Pergamon Press, New York, 1961, pp. 182–186.
6. Guthric, A., and R. K. Wakering, *Vacuum Equipment and Techniques*, McGraw-Hill Book Co., Inc., New York, 1949.
7. Redhead, P. A., *Errors in the Measurement of Pressure With Ionization Gages*, 1960 Seventh National Symposium on Vacuum Technology Transactions, Pergamon Press, New York, 1961, pp. 108–111.
8. Harding, John T., and Robert H. Tuffias, *The Cryogenic Gyro*, Technical Release No. 34–100, Jet Propulsion Laboratory, Pasadena, California, August 1, 1960.
9. Morelli, F. A., F. P. Fehlner, and C. H. Stembridge, *Effects of Ultrahigh Vacuum on "Bacillus Subtilis Variety Niger,"* Research Summary No. 36–14, Jet Propulsion Laboratory, Pasadena, California, May 1, 1962, pp. 1–4.
10. Buckley, D. H., and R. L. Johnson, *Gallium Rich Films as Boundary Lubricants in Air and in Vacuum to 10^{-9} mm Hg*, prepared for ASLE-ASME Lubrication Conference, Pittsburgh, Pennsylvania, October, 1962.
11. Bryant, Paul J., *Vacuum Technology—Present and Future*, Vacuum Technology, September, 1962.
12. Space Programs Summary 37–17, Vol. IV, for the period August 1–October 1, 1962, Jet Propulsion Laboratory, Pasadena, California.
13. Krieve, W. F., "Fission Electric Cells," *Research Summary No. 36–8*, pp. 80–81, Jet Propulsion Laboratory, Pasadena, California, May 1, 1961.
14. Wilson, Melvin N., Jr., Francis L. Baldwin, and Eric G. Laue, *The JPL 25-Ft. Diameter Space Simulator.* Institute of Environmental Sciences 1962 Proceeding, Chicago, Illinois, pp. 105–118.
15. *Major Space Breakthrough by National Research Corp.*, News Release, National Research Corp., Cambridge, Massachusetts, August 23, 1962.

65. Techniques for Laboratory Studies of Modern Magnetism

By Floyd B. Humphrey

DR. FLOYD B. HUMPHREY *is Research Group Supervisor in Guidance and Control Research Section of the Jet Propulsion Laboratory. In addition, Dr. Humphrey is a Senior Research Fellow on the California Institute of Technology Electrical Engineering Faculty. He was graduated with a B.S. in Chemistry from California Institute of Technology in 1950, and received an M.S. in Physics and Chemistry from the University of Minnesota in 1950–1951, and a Ph. D. in Chemistry from California Institute of Technology in 1956. A native of Greeley, Colorado, he is a member of the American Physical Society, Institute of Radio Engineers, and the AIEE.*

INTRODUCTION

The challenge of introducing modern electronics into space has opened a multitude of new problems and is, in many instances, breeding a new type of electronics. The influence is felt mainly in computer electronics, where computers are asked to make the many instantaneous decisions associated with all facets of a space mission. For unmanned missions, the problems are particularly severe since here missions lasting many years are contemplated. Magnetic devices are used as one of the main approaches for meeting this longevity challenge. They are particularly desirable for those missions of the future where a nuclear reactor is aboard the spacecraft, causing the associated high temperatures and radiation.

Thin magnetic films have been a fruitful vehicle for the investigation of this new type of magnetism. Compared to other magnetic structures, they require very little sample preparation and are generally ready for investigation immediately after fabrication. The equipment necessary for research is of moderate cost, and even the academic researcher can participate—in striking contrast to older types of magnetic research that required furnaces, rolling mills, and hours of sample preparation. This paper will be confined to a discussion of those techniques and instruments used in research into the magnetic character of thin films. From such investigations, the magnetic character of other structures can be inferred.

PREPARATION

The films are made by vacuum evaporation from permalloy. The useful compositions are from 15% iron, 85% nickel to 45% iron, 55% nickel. The thicknesses considered are from 100 to 5000 Å, with most consideration given to those of approximately 2000 Å. Usually the films are in the form of spots on a glass substrate. They are mirror-like and remain so for months without protection. When thicker than 150 Å, their electrical conductivity is as would be expected from bulk material before annealing (Ref. 1).

The evaporation technique most commonly used has been described by Blois (Ref. 2) and others (Ref. 3 and 4). A schematic diagram of the setup can be seen in Figure 65–1. Usually a zirconium or aluminum crucible is used to contain the melt. A charge of a few grams of either vacuum cast alloy or the proper propor-

666582 O—62——27

tion of vacuum cast nickel and iron can be used. When heated to approximately 1725° C by either a resistance or an induction heater, evaporation takes place at such a rate that condensation onto a substrate 10 cm away occurs at approximately 4000 Å/min. The magnetic characteristics of the final film depend upon evaporation rate. A shutter system, shown in Figure 65–2, is generally used to shield the substrate while the melt is heating to temperature. It is desirable to maintain constant melt temperature during the time the film is actually being formed. It is also possible to evaporate directly from a filament of tungsten, although most investigations use induction heating. Soft glass is the most common substrate, and microscope slides are generally used. They must be cleaned and kept free from dust. Optimum films are obtained when the substrate is heated to approximately 300° C. Usually a mask is placed in front of the substrate to limit the area of the film, as can be seen in Figure 65–2.

The entire system indicated in Figure 65–1 is contained inside a vacuum system, usually a standard system as shown in Figure 65–3. The pressure must be low enough to assure that the mean free path of the evaporated metal atom is long compared to the distance between the crucible and the substrate. Pressures between 10^{-3} and 10^{-6} mm Hg have been used.

One requirement peculiar to magnetic thin films is the necessity of establishing the direction of uniaxial magnetic anisotropy in the film by having a magnetic field in the plane of the substrate during evaporation and any subsequent anneal. The field in our system is provided by a pair of Helmholtz coils mounted outside the bell-jar. These are capable of supplying a field in excess of 50 Oe for an extended period of time.

The thickness of the film can be monitored by resistance which indicates the approximate thickness during evaporation. To obtain more detailed information about the evaporation, it is possible to use a micro-balance inside the vacuum system (Ref. 5). With the balance, the rate of evaporation and thickness can be determined and the temperature of the melt indicated. After the film is made, the thickness is usually measured optically or by X-ray fluorescence.

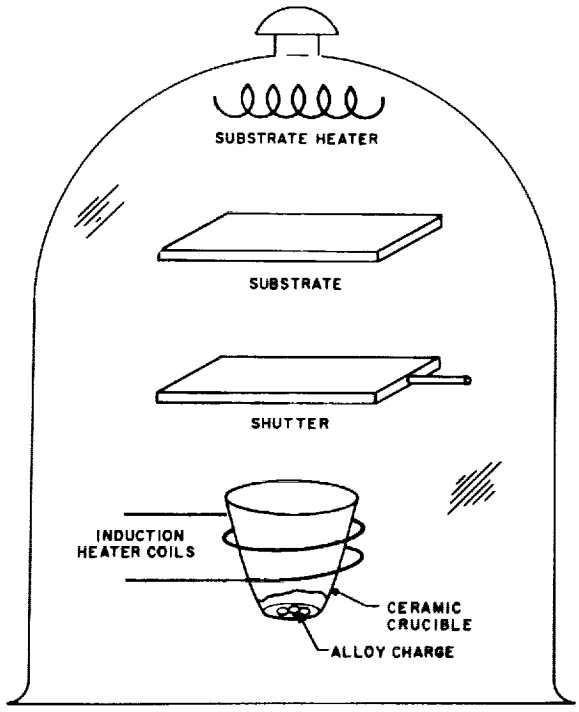

FIGURE 65–1.—Schematic of evaporation stand.

HYSTERESIS LOOP

The most common magnetic measurement is the magnetization hysteresis loop. Instruments such as the one described by Crittenden, et al (Ref. 6), and Oguey (Ref. 7) are very useful and have the magnetic sensitivity necessary to operate with extremely thin films. The loop is usually presented directly on the screen of a cathode ray oscilloscope at the rate of 60 cps or less. A typical loop can be seen in Figure 65–4. On the abscissa the magnetic induction H, which is proportional to the current through the driving coil, is plotted. The ordinate is the flux density B. The value of B for a very large drive, either positive or negative, is the saturation flux density B_s. The value of B for zero drive is the remanent flux density B_r. The squareness may be defined as B_r/B_s. The value of H for zero magnetization; that is, the value of the drive that will just demagnetize the sample, is called the coercive force H_c.

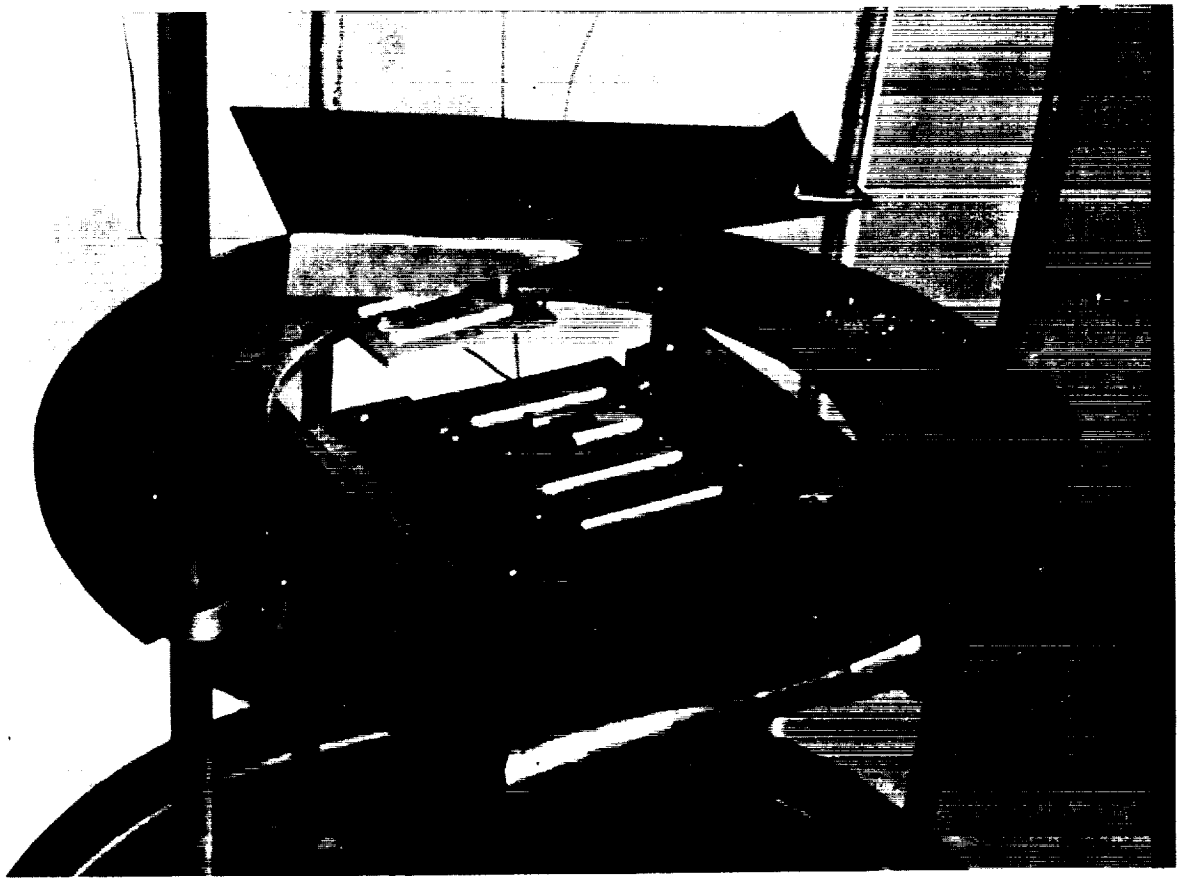

FIGURE 65–2.—Shutter system.

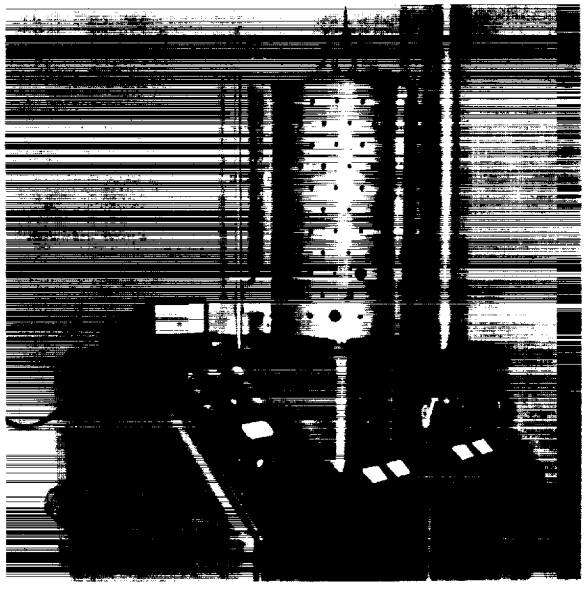

FIGURE 65–3.—Standard vacuum stand.

A photograph of our loop tracer is shown in Figure 65–5. The large coil pair cancel stray fields at the sample, a necessary procedure when working with thin films. The drive coils and pickup coils are smaller and can be seen in Figure 65–6. An operational amplifier provides the necessary integration. With a 1500 turn pickup loop and an open loop gain in the

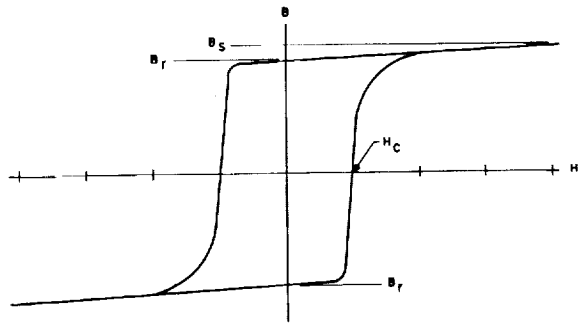

FIGURE 65–4.—Typical hysteresis loop.

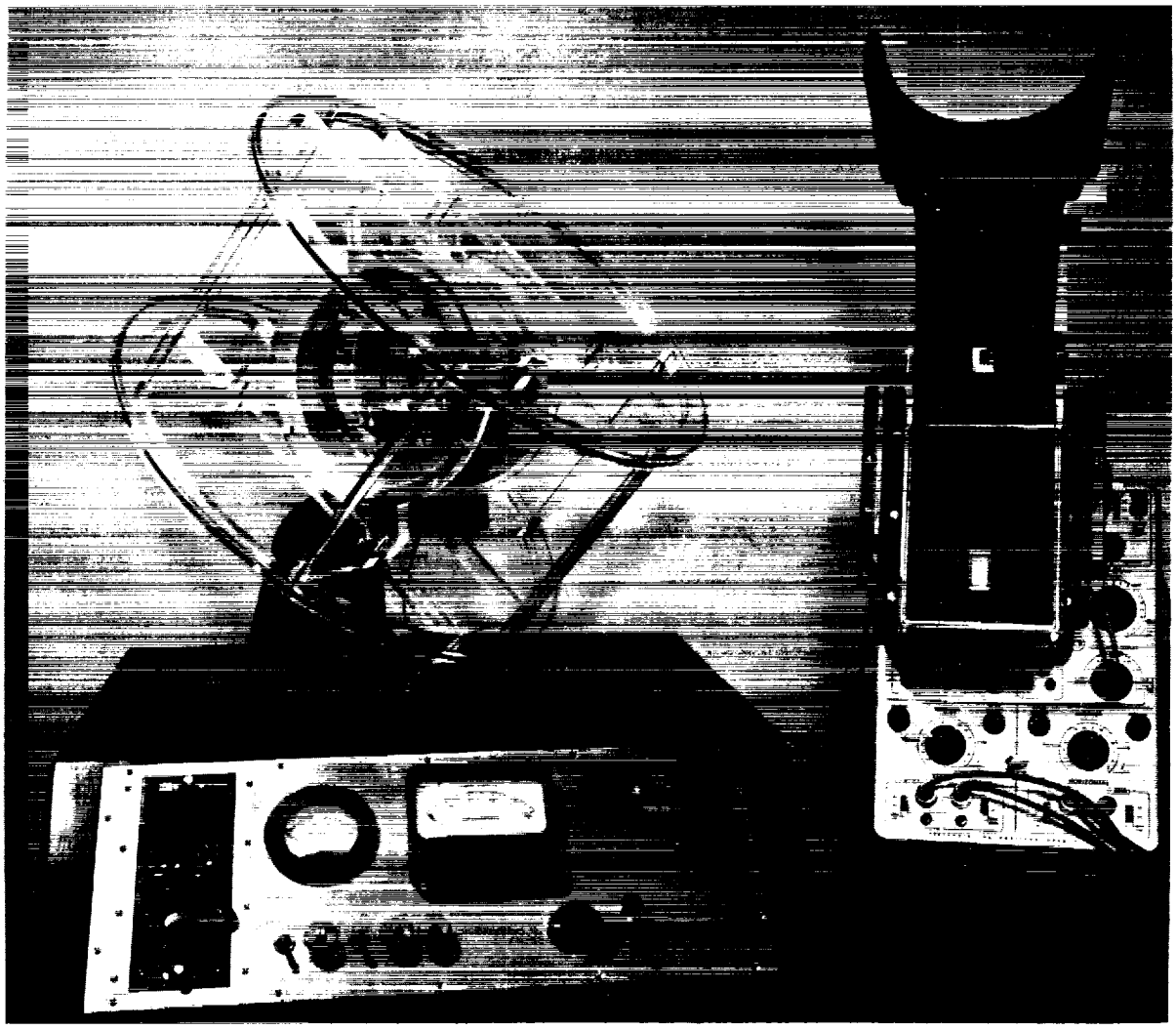

FIGURE 65-5.—Loop tracer.

amplifier of about 10^7, the minimum flux detectable is 10^{-3} maxwell. Trinagular drive is normally used at 17 cps. Manual control is also provided so that the field can be changed very slowly when the loops are steep.

A hysteresis loop taken along the easy axis of magnetization can be seen at the top of Figure 65–7. This figure was taken from a photograph of the oscilloscope face while sweeping the field very slowly. The Barkhausen pulses can be observed. Films typically have loops which are much squarer than those of ordinary magnetic material. In the center of Figure 68–7, taken as a double exposure, is the hard direction loop or transverse loop. The character of the loop is considerably changed when the drive and pickup are perpendicular to the easy direction of magnetization. The typical loops of Figure 65–8 were taken with increasing drive in this perpendicular condition. As mentioned previously these films all contain a uniaxial anisotropy. The mechanism for this anisotropy is not well understood. The effect of this, however, can be characterized by measuring the quantity usually called the anisotropy field H_k. With the film such that drive and pickup perpedicular to the easy axis, the drive current is adjusted to be so small that a single sloping line is seen on the oscilloscope, as in the upper loop of Figure 65–8. The slope of this

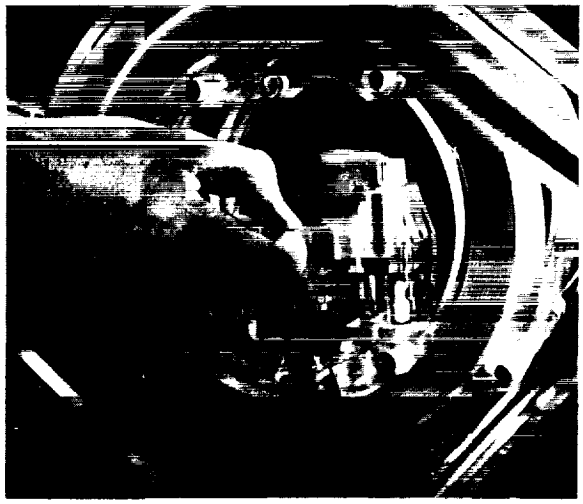

FIGURE 65-6.—Inner coils of loop tracer.

line is noted. The drive is then increased until the same is saturated as in the next loop of the Figure. The value of B_s for the sample is noted. H_k is defined as the field for which the extrapolated low drive slope intersects the value of B_s.

Torque Balance

For many years the magnetic torque balance has been an important instrument in the investigation of magnetic characteristics of materials. In 1937 H. J. Williams (Ref. 8) surveyed the usefulness of such an instrument for measuring the anisotropy constant, coercive force, and rotational hysteresis loses in magnetic materials. The evolution of the instrument continued gradually for over 20 years until R. F. Penoyer

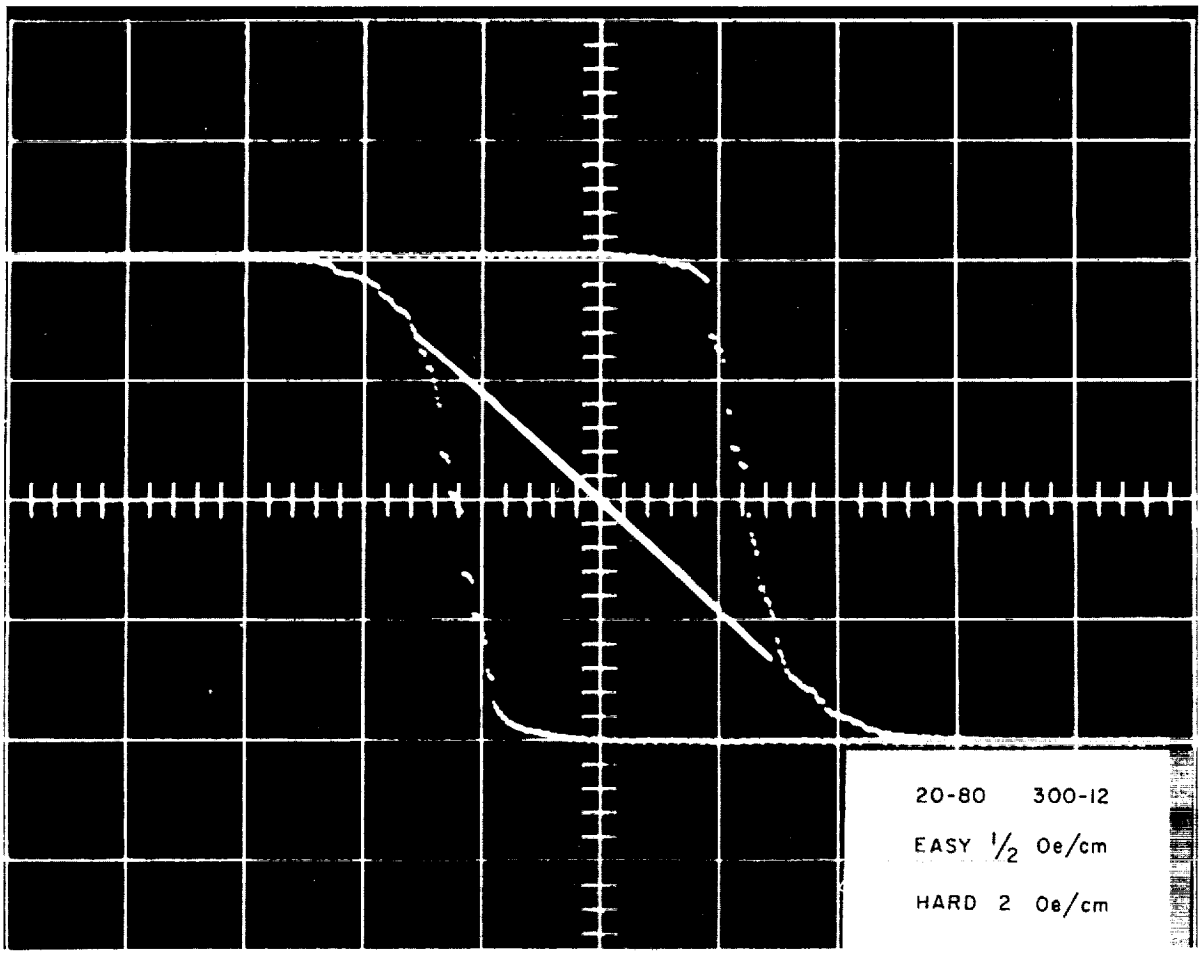

FIGURE 65-7.—Hysteresis loop.

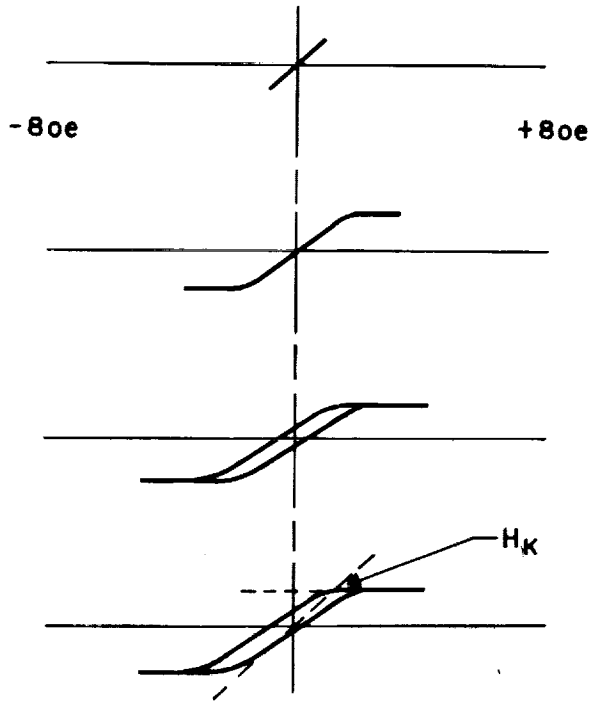

FIGURE 65-8.—Typical transverse loops.

(Ref. 9) incorporated electronics into the instrument to make it automatically self-balancing. E. L. Boyd (Ref. 10) increased the sensitivity of the automatic model and adapted it to the investigation of thin magnetic films as did W. D. Doyle (Ref. 11). Several others have adapted the manually-balanced torque meter for thin films (Ref. 12–16).

The instrument described here uses (Ref. 17) the principle of the Penoyer and Boyd instruments, but has a unique fused-silica suspension and servo-system that allows an increase in the sensitivity of about three orders of magnitude to 10^{-6} dyn/cm, with a resolving time of a fraction of a second. It is designed principally for the investigation of thin permalloy films and can measure the torque either perpendicular of parallel to the surface of the film. The saturation magnetization M_s, remanent magnetization M_r, anisotropy constant K, and coercive force H_c can be measured directly, allowing calculation of the anisotropy field H_K and the squareness.

The measurements of anisotropy field are of particular interest because the anomalous uniaxial anisotropy has continued to be an interesting and baffling phenomenon (Ref. 18). It is generally assumed, as was first thought by Smith (Ref. 19), that the classic Stoner-Wohlfarth model (Ref. 20) which was formulated to describe small single-domain particles, also describes the anisotropy in thin films. For a field in the plane of the film, the anisotropy can be defined in terms of energy (per unit volume) of the sample in the presence of a magnetic field as follows:

$$E=K \sin^2 \varphi - HM \cos (\alpha-\varphi)$$

where K is the anisotropy constant assuming uniaxial anisotropy, H is the magnetic field at some angle α from anisotropy axis, and M is the magnetization (per unit volume) of the sample at some angle φ from the anisotropy axis. At equilibrium $dE/d\varphi=0$ so that

$$MH \sin (\alpha-\varphi)=K \sin 2\varphi \qquad (2)$$

The torque ($L=\vec{M}\times\vec{H}$) per unit volume for this case is equal to

$$L=-MH \sin (\alpha-\varphi)=-K \sin 2\varphi \qquad (3)$$

where the minus sign indicates that the torque is in a direction of decreasing α. Depending upon the particular circumstances, as will be discussed below, the torque perpendicular to the plane of the film is a sensitive indication of the remanent magnetization or of the anisotropy.

For fields small compared to $4\pi M$ (so that the magnetization is in the plane of the film), another configuration is useful to measure the torque parallel to the plane of the substrate. For this case

$$L=-MH \sin \alpha \qquad (4)$$

where α is now the angle between the field and the substrate, and the torque is parallel to the plane of the film and perpendicular to the easy axis. If the easy axis is rotated so that it is parallel to the torsion axis (i.e., perpendicular to the field), Eq. (4) is applicable only for fields where $H \cos \alpha$ is greater than $2K/M$. For ($H \cos \alpha$) less than $2K/M$, the torque along the easy axis (z-axis) can be calculated in similar manner to be

$$L_z=\frac{M^2H^2}{4K} \sin 2\alpha \qquad (5)$$

Depending upon the particular situation, the torque observed parallel to the plane of the

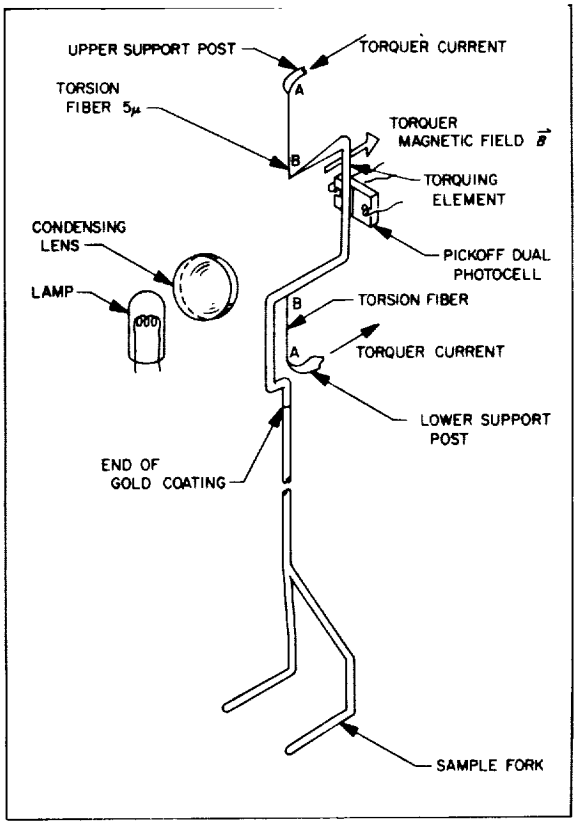

FIGURE 65–9.—Schematic of torquemeter.

film when a field is applied at some angle to the plane may be a sensitive measure of the magnetization M, the anisotropy field H_K, and the coercive force H.

The operation of torque balance can best be understood by referring to Figure 65–9. The shadow of the torquing element (B–B) caused by the lamp and condensing system falls on the dual photocell. The torquing element is in a uniform magnetic field as indicated, so that current through the element causes a torque about the axis defined by the torsion fibers. The output of the photocell is connected, through a high-gain servo amplifier, to the current through the torquing element, so that this output remains centered on the photo pickoff. The current is proportional to torque and can be measured as indicated in Figure 65–10. An auxiliary hanger, shown in Figure 65–11, allows measurement of torque along a torsion axis parallel to the plane of the substrate. For torques perpendicular to the plane, the sample is placed directly on the sample-carrying fork indicated in Figure 65–9. A photograph of completed assembly is shown in Figure 65–12. The earth-bucking cube coils and the rotating field coil can be seen.

Figure 65–13 shows a typical set of torque curves taken perpendicular to the plane of the film. These curves are from a film 40 Å thick, deposited in about 2 sec onto a glass substrate at 300° C. The composing is 76.2% nickel and 23.8% iron. A typical measurement parallel to the plane of the film using the auxiliary hanger is shown in Figure 65–14. Here the coercive force is measured. The details of these and other measurements made with the torque balance can be found in Ref. 17–21.

MAGNETIC DOMAINS

One of the more exciting static observations in magnetism is the direct observation of magnetic domains. The three methods that are in general use are the Bitter technique, the Kerr technique and the Faraday technique. The Bitter powder pattern technique (Ref. 22) consists of placing a colloidal solution of magnetite in water upon the carefully-prepared surface of the specimen. There are high field gradients at the wall caused by a divergence of the magnetization which attract the ferromagnetic magnetite. Usuing dark field or oblique illumination, the concentration of colloidal particles can be observed defining the walls. A thin film is a fine specimen for this experiment since its surface needs no preparation. This technique has been used extensively by Williams and Sherwood (Ref. 23). A sample of their results can be seen in Figure 65–15.

Another technique, utilizing the longitudinal magneto Kerr effect, was first used for films by Fowler, et al. (Ref. 24). This scheme allows optical observation of the domain rather than the walls. The arrangement can be most easily understood by considering Figure 65–16. Polarized white light is used to illuminate the sample at about a 60-deg angle of incidence. The reflected light passes through an analyzer and then through a simple lens system to the eye or a TV camera. The plane of polarization of the reflected light can be rotated a few degrees depending upon the direction of the field

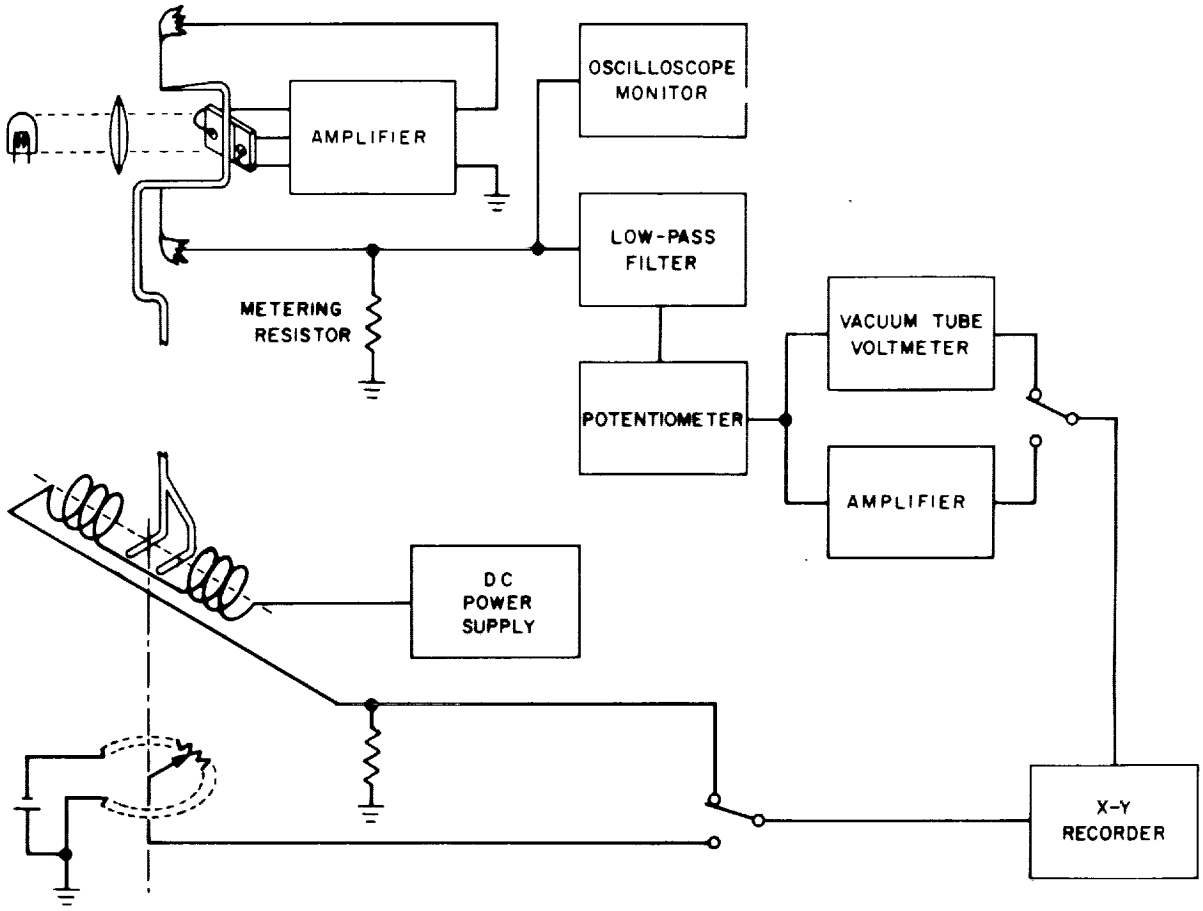

FIGURE 65–10.—Block diagram.

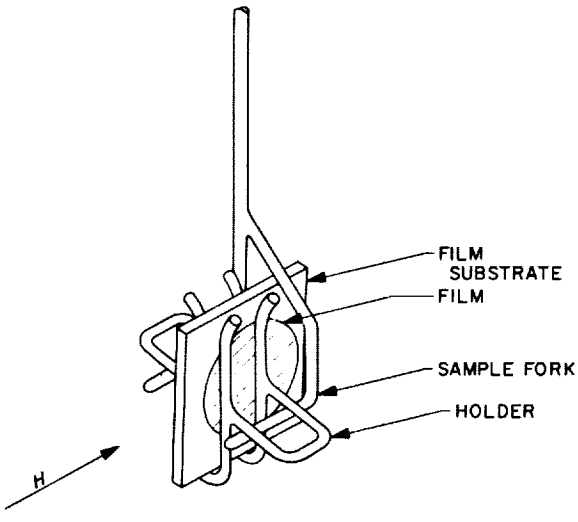

FIGURE 65–11.—Auxiliary hanger.

in the sample. Again nickel-iron films require no surface preparation, making this technique the most popular one for magnetic films.

A photograph of our equipment can be seen in Figure 65–17. It uses an Osram high-pressure mercury arc for illumination, Oland-Thompson prisms for polarization, and closed circuit television for observation. The television not only facilitates observation but increases contrast electronically. The cube coil system shown nullifies stray fields and establishes the necessary working fields used during the investigations. A photograph of some typical domain patterns is shown in Figure 65–18.

For very detailed observation where high magnifications are required, the Kerr effect loses

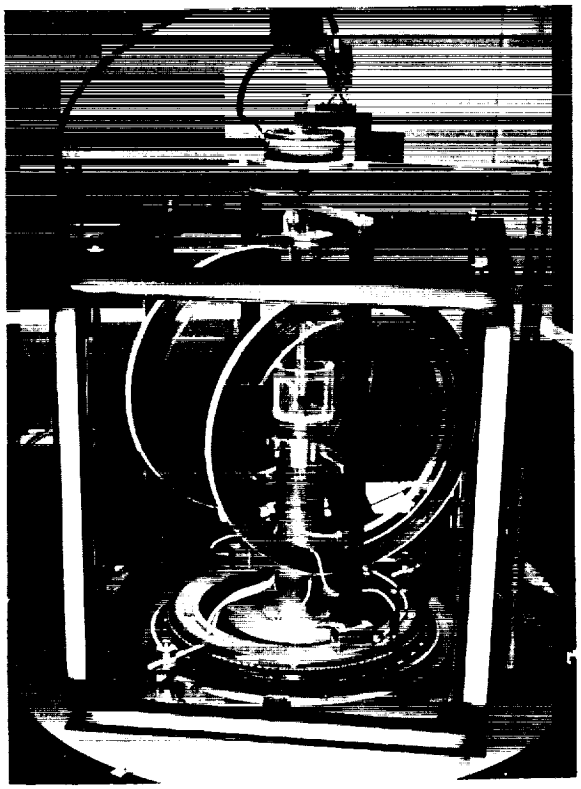

FIGURE 65–12.—Automatic torque balance.

contrast because of the very slight rotation. Either the Bitter technique must be used or, for films thinner than 700 Å, the Faraday effect can be utilized. The principle is essentially the same as before, except that now the light goes completely through the film at some angle, usually 45 deg. Interesting domain patterns result (Ref. 25), as can be seen in Figure 65–19.

DYNAMIC FLUX REVERSAL

The usual pulse experiment consists of saturating the sample with a field of about ten times the coercive force, and then reversing the magnetization by applying a step field pulse in the opposite direction. The reversal time τ_s is defined as the interval between the time when 10% of the total flux has reversed and the time when 90% of the total flux has reversed. The inverse of this reversal time can then be plotted as a function of the drive field H_c, as seen in Figure 65–20. It is possible to change the initial conditions by applying a dc field in the plane of the film and perpendicular to the drive field and, hence perpendicular to the easy axis of uniaxial anisotropy. Such a transverse field changes the reversal time for a given drive as is noted in Figure 65–20, where the transverse field H_T is included as a parameter. This behavior is unique for thin films made as described.

The equipment used for such a given experiment involves a number of compromises which depend on the specific requirements for the experiment. The general character of all the pulse equipment is the same, however. A drive field is required. The amplitude of the field must be constant and the same over the entire sample compared to the shortest time measured in the experiment. It must be possible to conveniently adjust the amplitude from point to point. The duration of the pulse does not matter as long as it is longer than the time being measured. The detection equipment must have a response time that is shorter than the times being measured and a sensitivity capable of detecting the very small flux changes associated with thin films. It is usually necessary to integrate since the flux rather than rate of change of flux is of interest.

Two types of field generation equipment are in general use. The first is the stripline pulser used when the ultimate field rise time is desired. Such a system is indicated schematically in Figure 65–21. A high-voltage power supply charges a length of coaxial cable to twice the voltage of the pulse desired through a series charging resistor. A relay with mercury wetted contacts discharges the line through a length of cable, hence through a stripline section to a termination. Generally, the relay is operated at 60 cps. The length of the cable has delay one-half the time length of the desired pulse. It should also have a center conductor with a resistance small compared to the impedance of the system or compatible with the voltage drop that can be tolerated. The value of the series charging resistor is a compromise between charging the cable completely and having the dc current though the relay small. Although the relay will close and allow a very high current (thousands of amperes), it will open only a few hundred milliamperes.

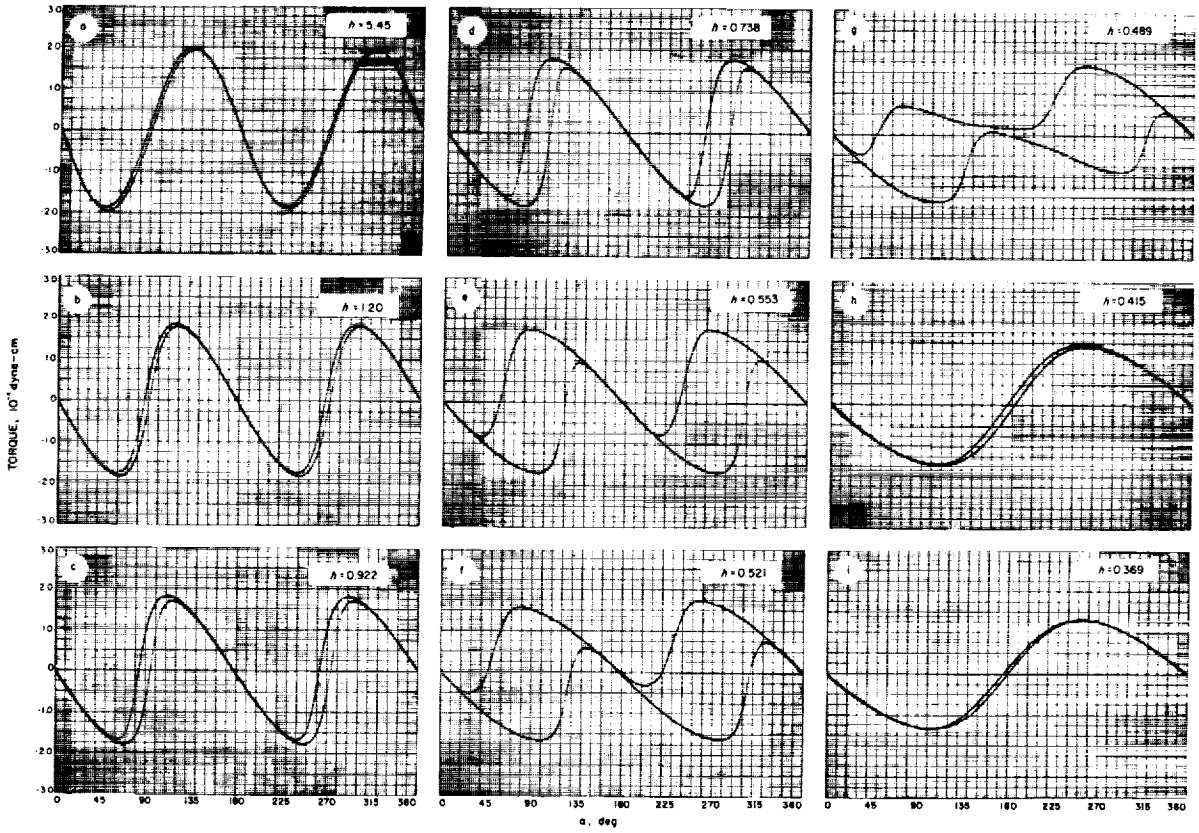

FIGURE 65–13.—Typical set of torque curves.

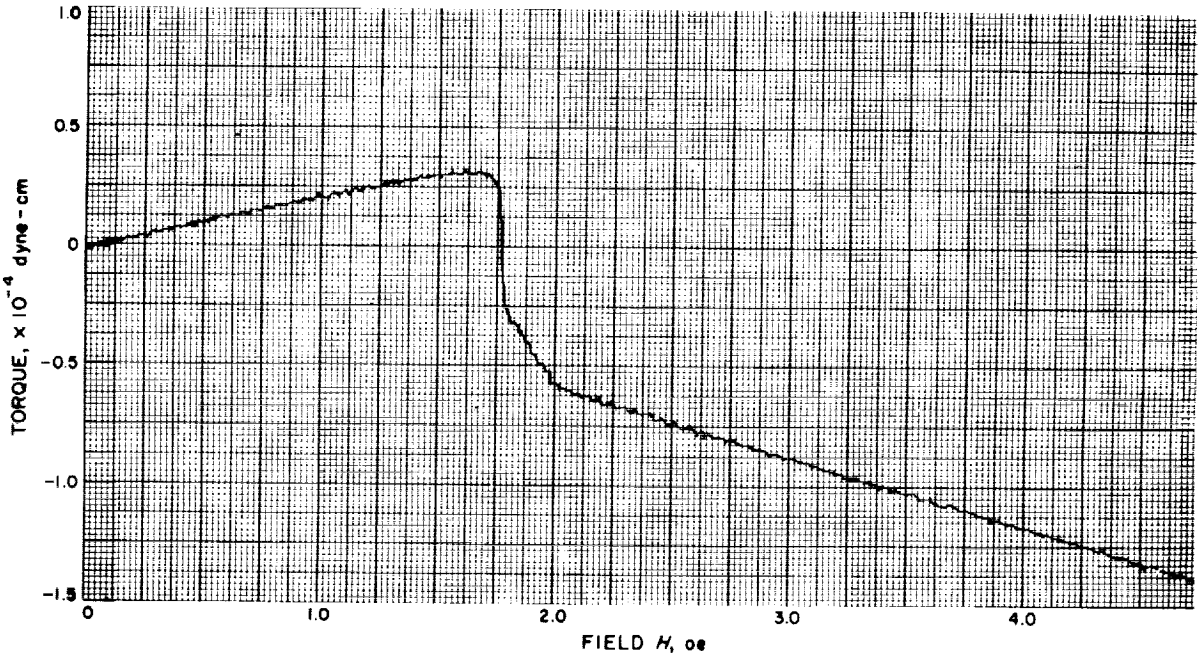

FIGURE 65–14.—Measurement of the coercive force.

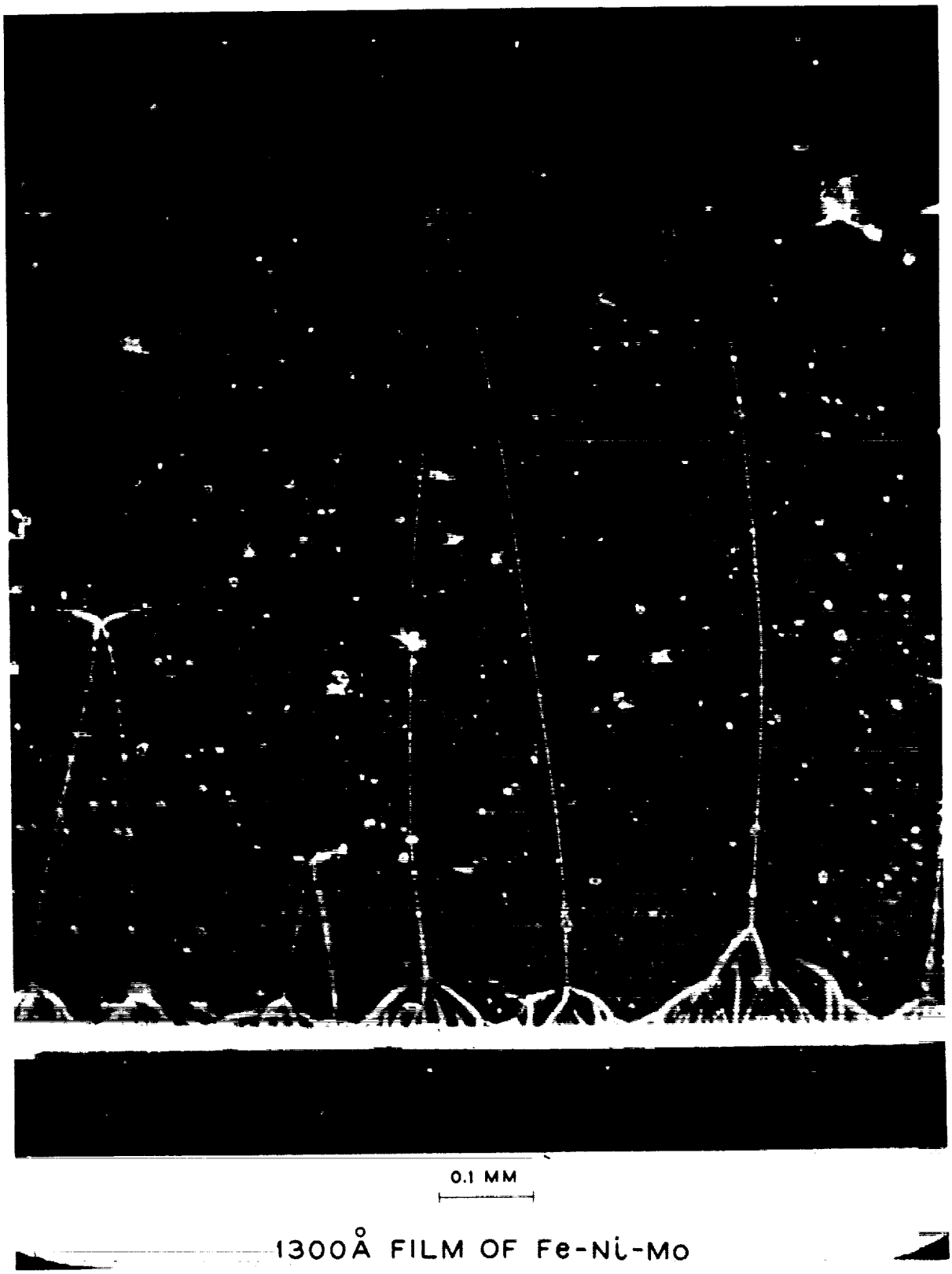

FIGURE 65–15.—Bitter powder pattern.

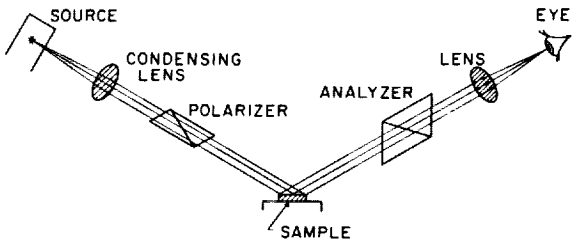

FIGURE 65–16.—Schematic of Kerr effect apparatus.

The relay is usually in a coaxial holder which can be fabricated in a number of straightforward ways. The relay body is a commercial item. It will generally hold off approximately 4000 v. Operating at 60 cps is within the capabilities of most relays.

The stripline affords a convenient transmission line section of the type where the magnetic field is uniform and accessible. A typical section is shown in Figure 65–22. The dimensions used depend upon the impedance in a straightforward way (Ref. 26). The pickup must be insensitive to the change in field brought on by the onset of the pulse. Generally two loops are used connected in series opposition, as shown in Figure 65–23. Since the use of the stripline presupposes interest in fast events, normally only single turn coils are used, connected as in Figure 65–23. The series resistors prevent the loops from being a shorted turn.

It is usually most convenient to integrate immediately with either an RC integrator or an electronic integrator. Since again frequency response is presumed to be important, the RC integrator is the easiest. The voltage out is very small, however, putting a severe sensitivity requirement upon the rest of the detection equipment. A transistorized Miller integrator has been constructed (Ref. 27) which considerably simplifies the matter. It has a response time of 3 nsec and a decay time of 10 microsec with a capacity of 30 mv-microsec.

The rest of the detection system depends upon film thickness. Distributed amplifiers (HP 460 A and B) can be used or transistorized amplifiers with slightly better response time. The voltage rise can then be observed on a sampling oscilloscope. The ultimate in sophistication can be obtained by using the Tektronix 567 digital readout where the rise time is automatically recorded with nixie tubes.

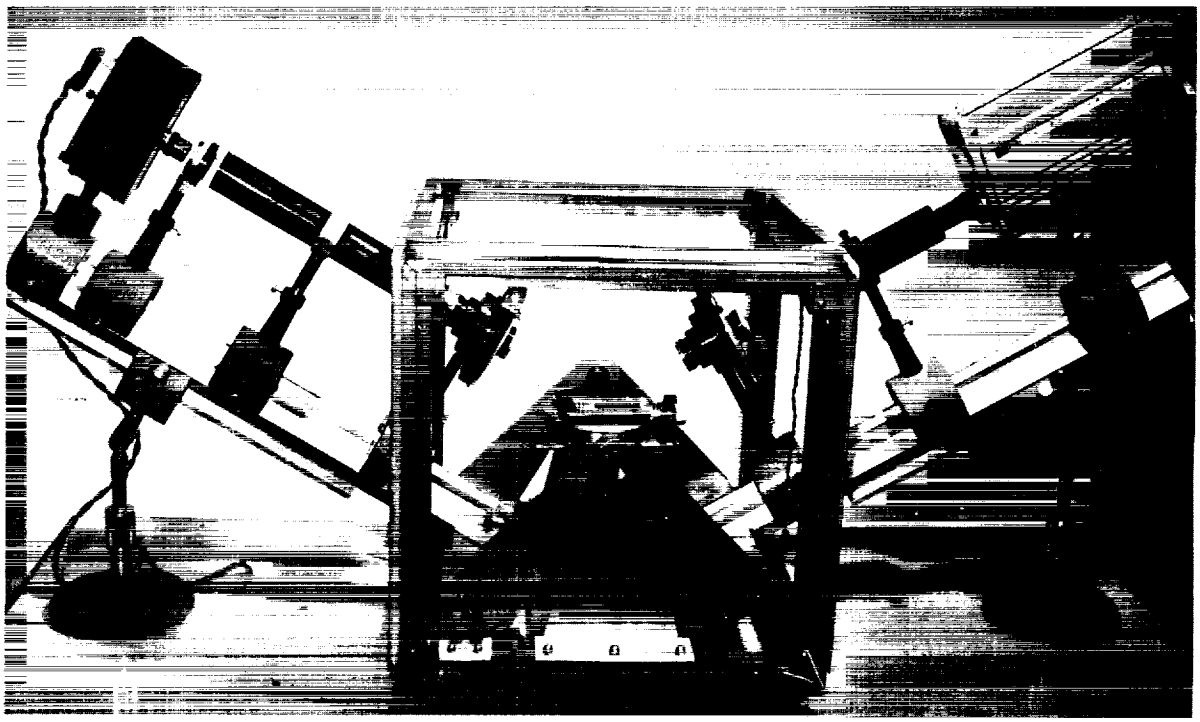

FIGURE 65–17.—Kerr magneto optic domain viewer.

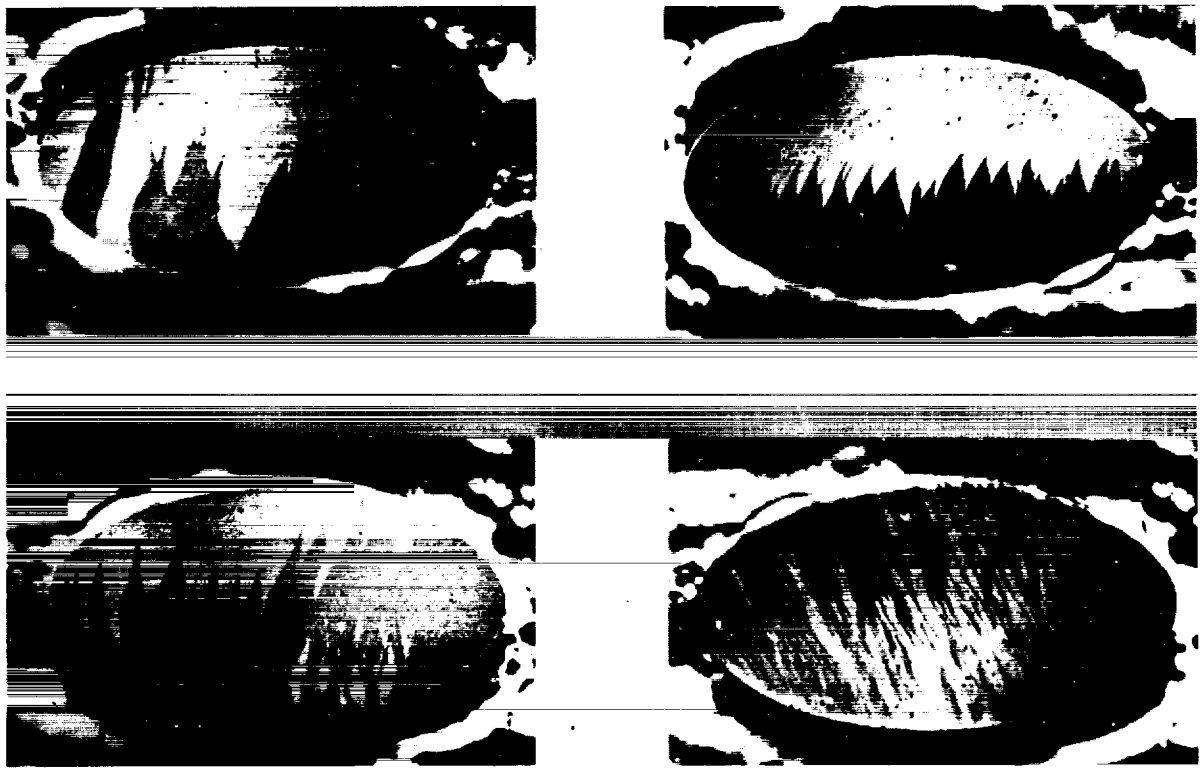

FIGURE 65–18.—Typical domain patterns.

A photograph of the stripline and setting coils is shown in Figure 65–24. Various other coils provide the logical fields for nullifying stray fields, providing the transverse fields, etc.

By not demanding the fastest system, the detection problem can be eased. Multiturn pickup loops can be used relieving the amplifier problem. Standard vacuum tube pulsers can feed distributed transmission lines to give the field. One such setup can be seen in Figure 65–25. The 20-turn pickup and distributed solenoid can be used for films as thin as 100 Å to investigate the velocity of Néel walls (Ref. 28). The entire electronics setup is illustrated in Figure 65–26.

Of course, in the investigation of the dynamics of flux reversal, it is not enough to just measure the switching time. There are many pulse experiments that can be used to infer the reversal mechanism. The interrupted pulse experiment (Ref. 29) is a particularly important one to identify domain wall motion. The simultaneous observation of the longitudinal and transverse loops (Ref. 30) is particularly important in the identification of uniform rotations. These experiments, however, are all performed using the same type of equipment as discussed previously.

CONCLUDING REMARKS

In summary, it is proposed that investigations in modern magnetism are both interesting and timely. Participation can be achieved with a limited budget. The most important instruments in a laboratory devoted to such a study are a loop tracer, a torque balance, a Kerr domain viewer, and a pulse flux reverser.

FIGURE 65–19.—Faraday effect patterns.

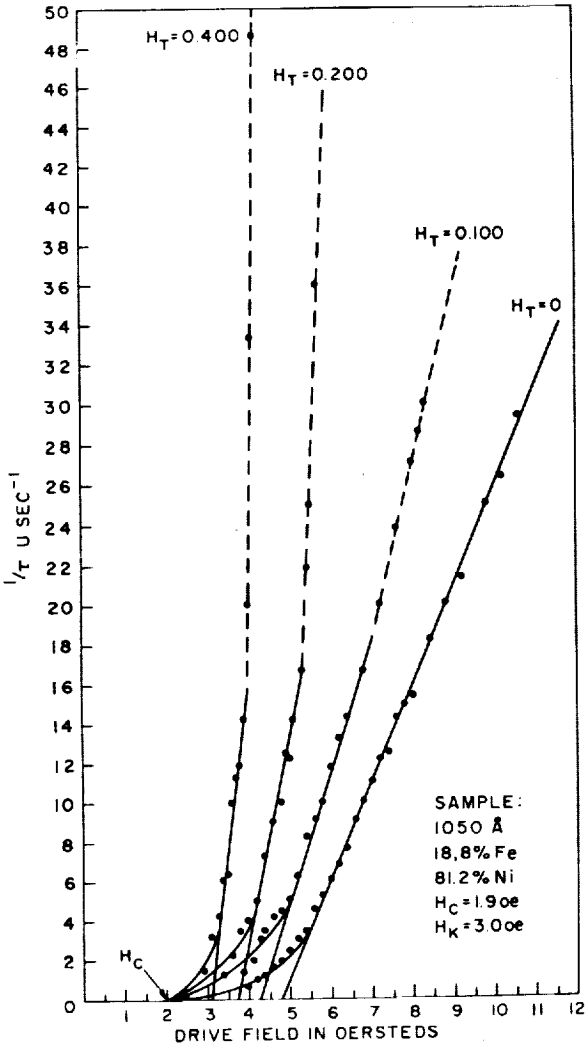

FIGURE 65–20.—$1/\tau$ vs. H.

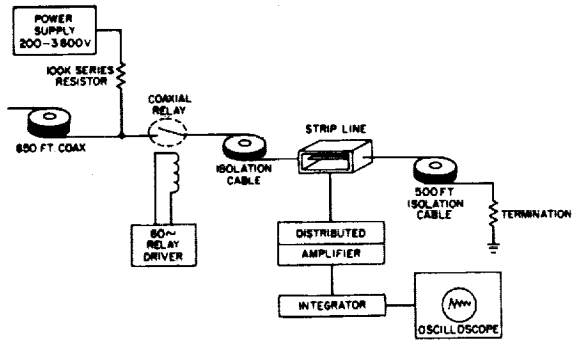

FIGURE 65–21.—Block diagram of stripline pulser.

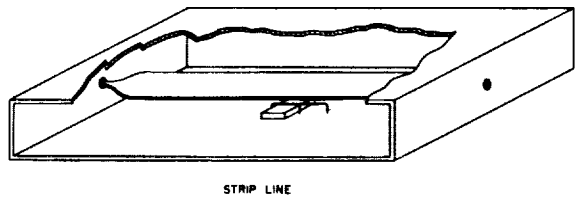

FIGURE 65–22.—Stripline cutaway.

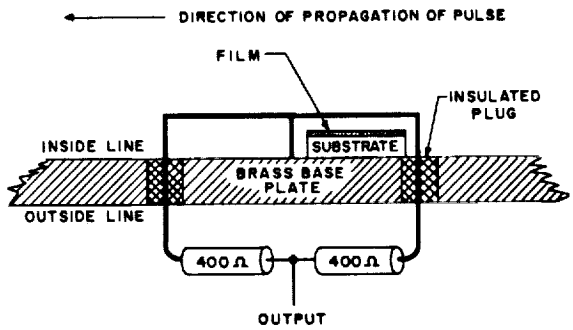

FIGURE 65–23.—Loops in stripline.

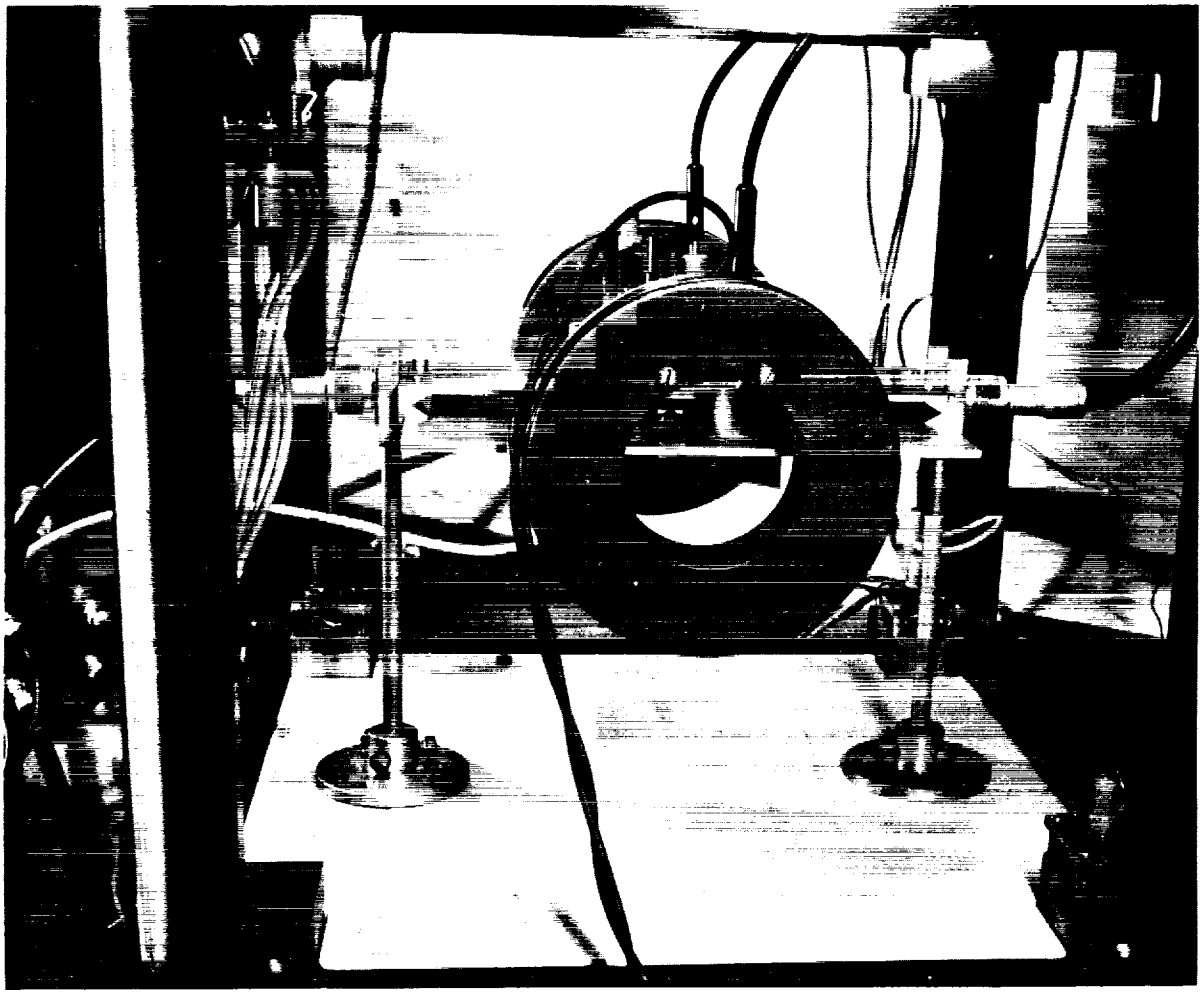

FIGURE 65–24.—Stripline.

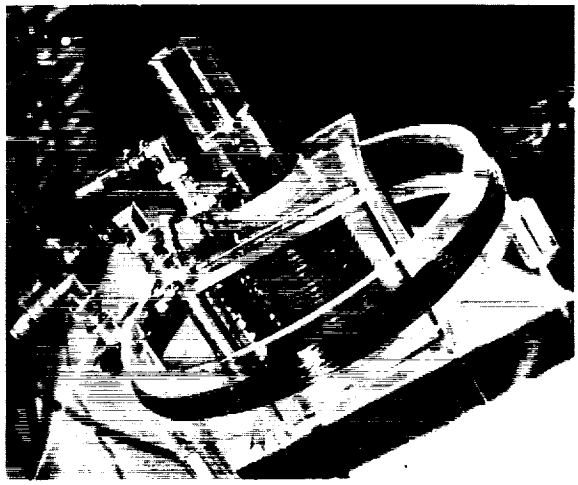

FIGURE 65–25.—Multiturn pickup and distributor solenoid.

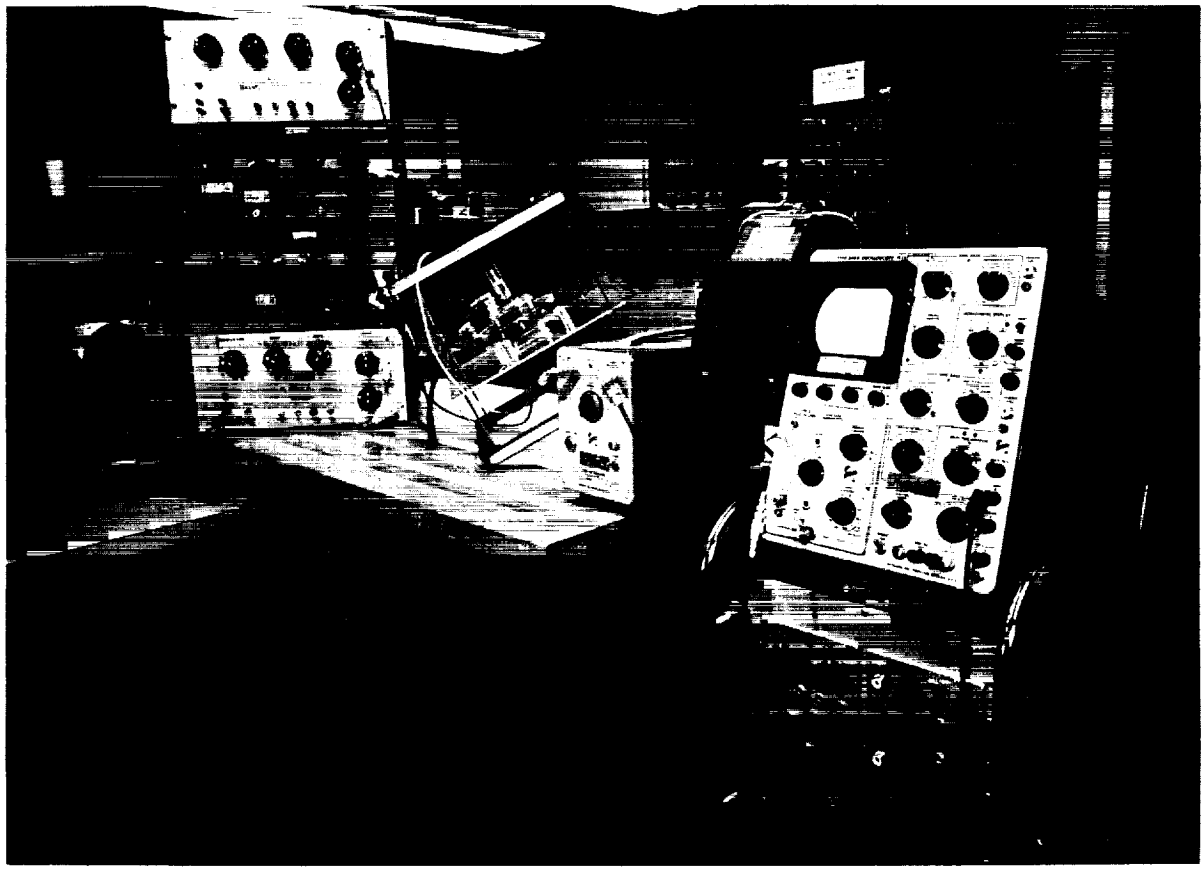

FIGURE 65–26.—Electronics for observing very thin films.

REFERENCES

1. HUMPHREY, F. B., F. W. REYNOLDS and G. R. STILLWELL, Transactions Vacuum Society Symposium 1958, Pergamon Press, p. 204.
2. BLOIS, M. S., JR., J. Apply. Phy., 975 (1955).
3. CRITTENDEN, JR., E. C., and R. W. HOFFMAN, Rev. Mod. Phys. *25*, 310 (1953).
4. CONGER, R. L., and F. C. ESSIG, Phy. Rev. *104*, 915 (1956).
5. HOUDE, A. L., Proceedings of Third Symposium on Vacuum Balance Techniques, Los Angeles, Oct. 31, 1962, to be published.
6. CRITTENDEN, E. C., A. A. HUDIMAC and I. R. STROUGH, Rev. Sci. Instru. *22*, 872 (1951).
7. OGUEY, H. J., Review of Scientific Instruments *31*, 701.
8. WILLIAMS, H. J., Rev. Sci. Instru. *8*, 56 (1937).
9. PENOYER, R. F., Rev. Sci. Instru. *30*, 711 (1959).
10. BOYD, E. L., IBM J. Res. Devel. *4*, 116 (1960).
11. DOYLE, W. D., J. E. RUDISILL, and S. SHTRIKMAN, J. Appl. Phys. *32*, 1795 (1961).
12. TAKAHASHI, M., et al., J. Phys. Soc. Japan *14*, 1959 (1959).
13. NEUGEBAUER, C. A., Phys. Rev. *116*, 1441 (1959).
14. GRAHAM, JR., C. D., and J. M. LOMMEL, Proc. Int. Conf. on Magnetism, Koyoto, 1961.
15. ANDRA, W., et al, Naturwissenschaften *46*, 257 (1959).
16. REINCKE, W., Z. Physik *137*, 169 (1954).
17. HUMPHREY, F. B., and A. R. JOHNSTON, Technical Report No. 32–321, Jet Propulsion Laboratory, Aug. 1962.
18. TAKAHASHI, M., J. Appl. Phys. *33*, 110 (1962).

666582 O—62——28

19. SMITH, D. O., Conference on Magnetism and Magnetic Materials, Boston, 1956. (AIEE Special Publication, Feb. 1957) p. 625.
20. STONER, E. D., and E. P. WOHLFARTH, Phil. Trans. Roy Soc., Londan, *240A*, 599 (1948).
21. HUMPHREY, F. B., and A. R. JOHNSTON, Rev. Sci. Instru. in press.
22. WILLIAMS, BOZORTH, and SHOCKLEY, Phys. Rev. *75*, 155 (1949).
23. WILLIAMS, H. J., and R. C. SHERWOOD, J. Appl. Phys. *28*, 548 (1957).
24. FOWLER, JR., C. A., E. M. FRYER and J. R. STEVENS, Phys. Rev. *104*, 645 (1956).
25. HOUDE, A. L., J. Appl. Phys. *32*, 1234 (1961).
26. Symposium on Microwave Strip Circuits, IRE Transactions, Vol. MTT-3 No. 2, March 1955.
27. MARSHALL, J. H., Space Programs Summary No. 37–17, Vol. IV, Jet Propulsion Laboratory, Oct. 1962.
28. COPELAND, J. A., and F. B. HUMPHREY, J. Appl. Phys. in press. (1962 Magnetics Conference Supplement.)
29. HAGEDORN, F. B., J. Appl. Phys. *30*, 254S (1959).
30. DIETRICH, W., W. E. PROEBSTER and P. WOLF, IBM J. of Res. and Devel. *4*, 189 (1960).

66. Generation of Magnetic Fields by Flux Compression in Superconductors

By Daniel D. Elleman

DR. DANIEL D. ELLEMAN, *Senior Scientist in the Physics Section of Jet Propulsion Laboratory, was born in Lancaster, Ohio. A graduate of Ohio State University, he received the B.S. in Engineering Physics and the M.S. in Physics in 1955 and the Ph. D. in Physics in 1959. Dr. Elleman holds membership in the American Physical Society and Sigma Xi.*

INTRODUCTION

The possibility of producing and carrying intense magnetic fields in space probes offers a solution to many problems encountered in space flight. A few of the obvious applications of magnetic fields are: plasma confinement for power generation and propulsion systems, magnetic shielding of astronauts, particle analyzers, bubble and cloud chambers, and magnetic resonance experiments. The utilization of these devices is feasible only if the power consumption and weight of the device are of a reasonable size for space probes.

The discovery (Ref. 1–4) of high critical field superconductors such as Nb_3Sn and Nb_2Zr has greatly stimulated interest in the possible production of very high field, large volume, superconducting solenoids (Ref. 5–7). Unfortunately, these high critical field superconductors do not have exceptionally high critical current density characteristics, $J \approx 10^5$ amp/cm^2. Furthermore, the manufactured superconducting wires must be rather small in diameter, 10–20 mil, because of the metallurgical properties of the superconductor. Another problem in wire wound solenoids arises from the introduction of heavy copper bus leads into the helium bath which produces a large heat leak into the helium bath. These difficulties make it necessary to construct the superconducting solenoid with small diameter wire which results in small energizing currents, 10–20 amps, for the solenoid. Therefore, a many turn solenoid must be wound in order to obtain the large ampere turns required for the intense magnetic field. It is immediately obvious that to produce magnetic fields of even intermediate sizes, such as 1 liter, would require many thousand meters of superconducting wire. In this paper, we describe an alternate method in which persistent currents are induced in a block of superconducting material so as to trap and then compress a large magnetic field within holes in the superconductor.

Flux Compression

It is a well known fact that when a multiply connected superconductor is cooled below its critical temperature in the presence of an external magnetic field the flux inclosed by the superconductor is trapped and remains constant even when the external magnetic field is reduced to zero (Ref. 8). Thus, if a superconducting cylindrical shell were placed in a magnetic field B_o, with the field parallel to the axis of the shell, then cooled below the critical temperature, the field B_o would be trapped in the

volume inclosed by the shell, and the field would remain trapped for an indefinite length of time (Ref. 9). In speaking of such a system, it is best to mention that the total magnetic flux trapped, ϕ_o, and the magnetic field remain constant only so long as the cross sectional area normal to the field does not change. It is easy to see that if it were possible to decrease the cross section available to the trapped flux the magnetic field would correspondingly be increased.

Figure 66–1 shows a block of Nb_3Sn 6.0 cm in diameter, 2.60 cm thick, and with two holes 2.30 cm diameter and 1.00 cm diameter drilled through the block. As an experiment to test the feasibility of compressing magnetic flux, this block was placed in the magnetic field of a copper wound solenoid 12 in. diam and 36 in. long, with the axis of the cylindrical holes in the block parallel to the magnetic field of the solenoid. A dewar system was constructed to cool the block below its critical temperature, 18° K, with liquid helium. In the experiment, the magnetic field was first turned on to a value B_o, and then the superconducting block was cooled with liquid helium and the magnetic field of the solenoid reduced to zero. Thus the field B_o or the flux ϕ_o was trapped in the two holes in the block; next the superconducting cylindrical piston, 2.220 cm in diameter, shown in Fig. 69–1, was inserted into the larger hole, hole A, in the block. The insertion of the piston compressed the flux ϕ_o into a smaller cross sectional area and thus gave an increase in the magnetic field measured in the small hole, hole B (Ref. 10 and 11).

If one assumes that the total trapped flux ϕ_o in the superconducting holes remains constant both before and after the piston is inserted into hole B, then

$$B_a = B_o\left[\frac{A_a + A_b}{A_a + (A_b - A_p)}\right] \qquad (1)$$

where B_a is the final field measured in hole A, A_a is the cross sectional area of hole A, A_b is the cross sectional area of hole B, and A_p is the cross sectional area of the piston. It is obvious from Eq. (1) that a very large magnetic field may be produced from a relatively small initial field merely by building a flux compressor with both hole B and the piston very large compared to hole A.

It is of course advantageous to trap as large an initial flux as possible. Making the field B_o of the copper solenoid larger will accomplish this, but can become very difficult for larger fields. A more convenient method of trapping a large flux is to place soft iron rods through holes A and B while the solenoid is on and before the superconducting block is cooled blew its critical temperature. The iron rods give a low reluctance path for the flux and thus increase the total flux through the holes in the block. After the superconducting block is cooled, the magnetic field of the solenoid can be turned off, then the iron rods can be withdrawn and the superconducting piston inserted into hole B. Using a technique similar to this, fields of 23.5 Kgauss have been produced with superconductors made of Nb_3Sn. If attempts are made to compress magnetic fields larger than 23.5 Kgauss, the superconductor goes normal, the magnetic flux leaks out of the holes in the block, and the field decays very rapidly to a value of only 2 to 5 Kgauss.

A Cyclic Flux Pump

As was shown above, the compression ratio obtained by flux compression is the ratio of the cross-sectional area available to the trapped flux before the superconducting piston is inserted, to the cross-sectional area available to the trapped flux after the piston is inserted. Therefore, in order to produce a high field in a large working area, it is necessary to have a very large compression chamber and piston. It is obvious that this arrangement can become extremely cumbersome. This troublesome requirement can be alleviated, however, by the addition of two superconducting valves to a compressor similar to the one described above. This makes it possible to obtain a large increase in the magnetic field without a very large compression chamber.

Figure 66–2 shows a picture of a cyclic superconducting flux pump fitted with two superconducting valves. The flux pump is constructed from a block of 99.6% niobium, 1.90 cm thick and 4.14 cm in diameter. There are two large cylindrical holes drilled through the block, one of 0.96 cm diameter, the compression chamber,

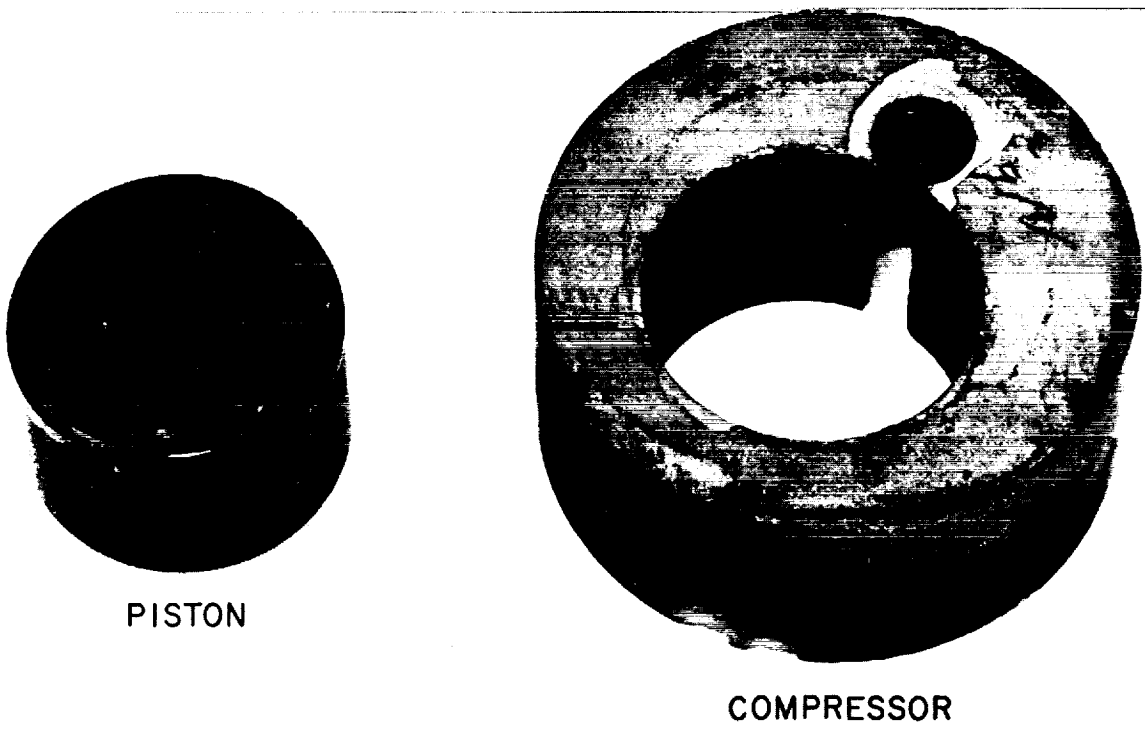

FIGURE 66–1.—A Nb_3Sn superconducting flux compressor and piston.

and the other hole 2.38 cm diam, the experimental or probe chamber. In addition, very small holes are drilled into the wall which separates the two chambers, and also in the outside wall of the compression chamber. Nichrome heating wires are placed in these small holes.

When a small voltage is applied to these heating wires, the temperature of the niobium is raised above the critical temperature and the niobium cylinder 2.12 cm long and 0.89 cm diam changes from the superconducting state to the normal state. The two superconducting valves can, therefore, be open or closed to let magnetic flux into or out of a particular chamber. A niobium cylinder 2.12 cm long and 0.98 cm diam is used as a superconducting piston to compress the flux in the compression chamber. The sequence of operation of the valves and the piston is the following: the entire system is brought to the superconducting state with liquid helium in the presence of an external field B_o, with both valves closed (superconducting), and the piston withdrawn from the compression chamber. The superconducting piston is then inserted into the compression chamber and the flux which was trapped in the compression chamber is compressed into the narrow annular region between the walls of the chamber and the piston to produce the resulting magnetic field

$$B=B_o\left(\frac{1}{1-\frac{A_p}{A_c}}\right)$$

where A_p is the cross-sectional area of the piston and A_c is the cross-sectional area of the

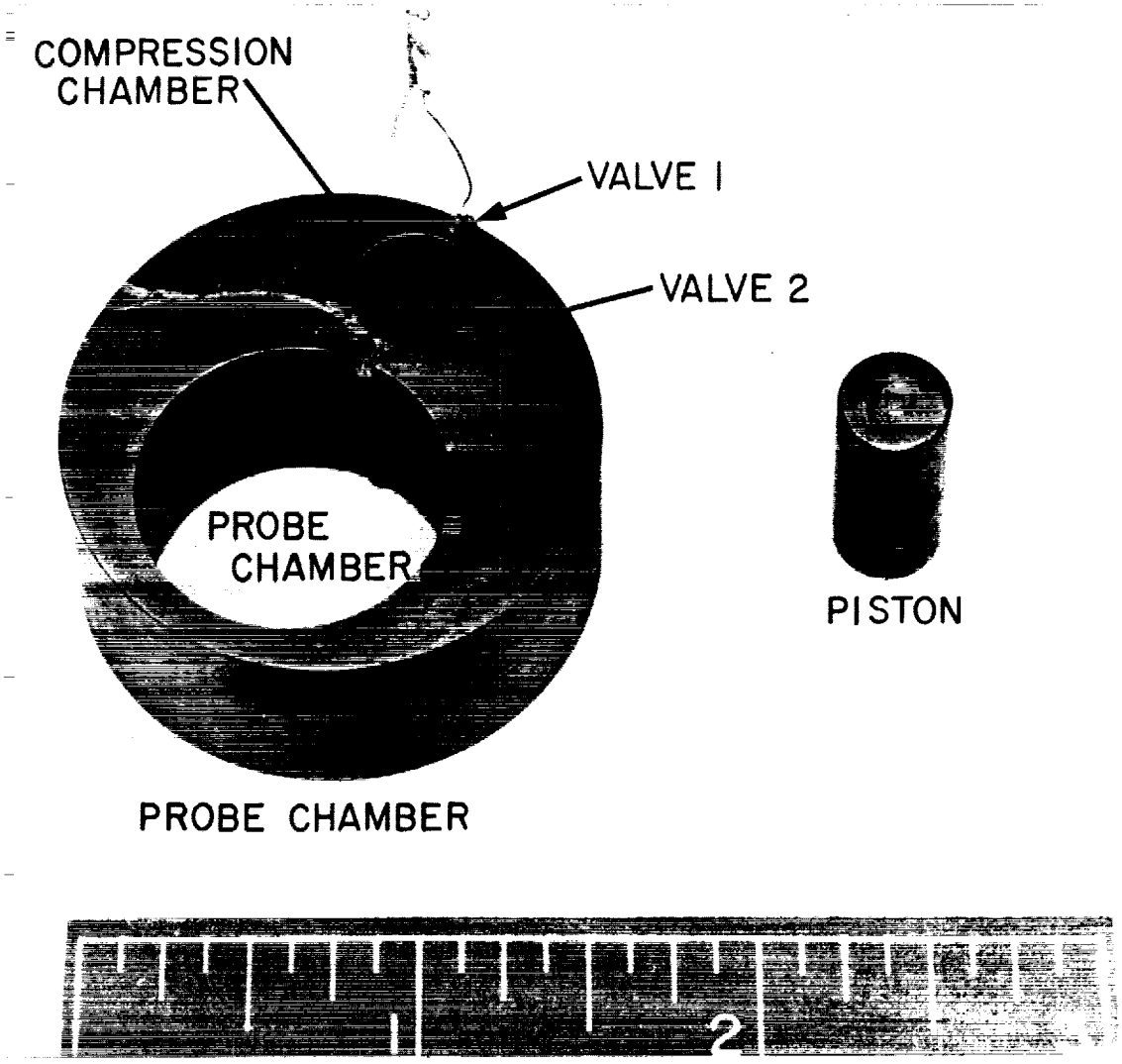

FIGURE 66–2.—A niobium superconducting cyclic flux pump and piston.

compression chamber. Valve 2 is then opened to enable the compressed flux to enter the probe or experimental chamber. (Actually, the flux is shared by the probe chamber and the annular region between the compressor wall and the piston). Valve 2 is then closed, isolating the two chambers, the piston is withdrawn from the compression chamber, and valve 1 is then opened. When valve 1 is opened, more magnetic flux from the ambient field enters the compression chamber; valve 1 is then closed, trapping this flux in the compression chamber. The piston is again inserted and the cyclic operation is repeated. With the completion of each cycle, the flux within the probe chamber increases until the magnetic field within the probe chamber is identical to that in the compression chamber during the compression phase. Thus, the maximum field that can be produced in the probe chamber is given by Eq. (2).

Figure 66–3 shows the results for several such experiments carried out in different external fields with the 99.6% niobium flux pump. Additional experiments have been performed with cyclic Nb_3Sn flux pumps, which obtained a field of 10 Kgauss. This field is less than was anticipated because of flux penetration into the walls of the superconductor.

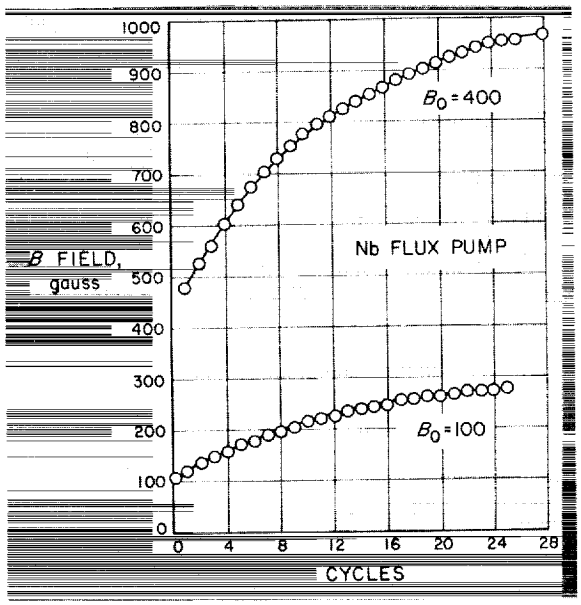

FIGURE 66–3.—A plot of magnetic field in probe chamber vs. cycles of operation for niobium flux pump.

A flux pump was also constructed out of two coils of 10 mil Nb_3Zr wire as is shown in Fig. 66–4. The coils were 1.2 cm in diameter and 4 cm in length, the superconducting piston was a 1.0 cm diam niobium cylinder 5 cm long. This flux pump was operated in a manner similar to the block of niobium pump. The results are shown in Fig. 66–5.

The Nb_3Zr flux pump has been operated as a "magnetic vacuum pump", that is, to pump magnetic flux out of the probe chamber. This was accomplished by merely changing the sequence of opening and closing the valves. The

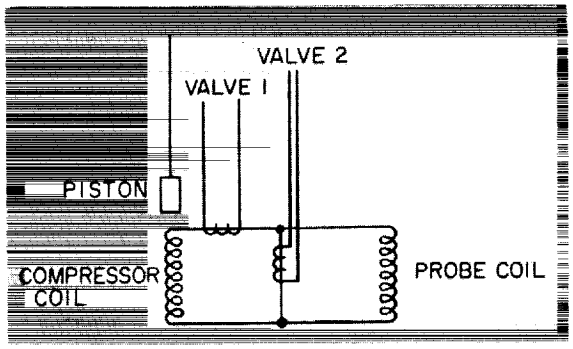

FIGURE 66–4.—A Nb_3Zr coil cyclic flux pump.

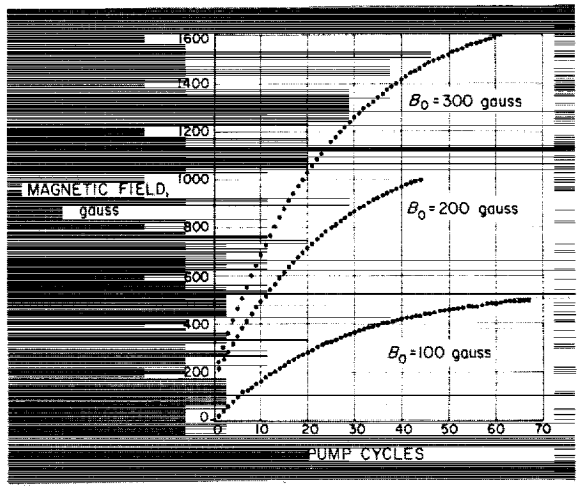

FIGURE 66–5.—A plot of magnetic field in probe coil vs. cycles of operation for Nb_3Zr flux pump.

Z component of the trapped field (the component along the axis of the coil) was pumped down from approximately 600 milligauss (the Earth's field in the laboratory) to 0.2 milligauss. Figure 66–6 shows a plot of Z component of the magnetic field vs. cycles of operation. The 0.2 milligauss field was extremely stable and showed changes of less than 10^{-3} milligauss when the field external to the coil was varied several gauss.

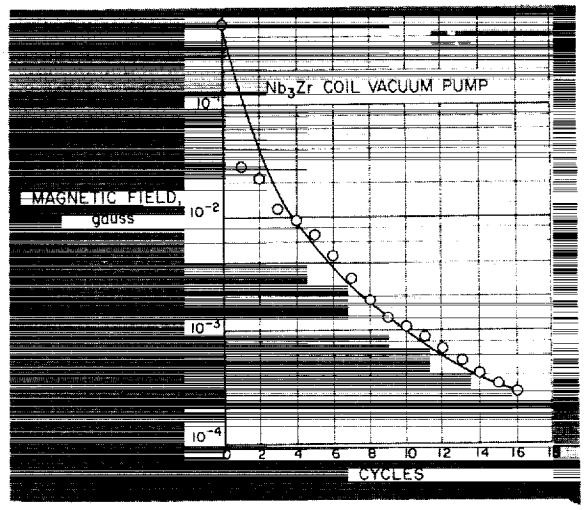

FIGURE 66–6.—A plot of magnetic field in probe coil vs. cycles of operation for Nb_3Zr "vacuum pump."

Penetration of Magnetic Flux Into Nb_3Sn

A superconducting flux compressor, similar to the one described above, has been used to measure the penetration of magnetic flux into the superconductor Nb_3Sn (Ref. 12 and 13).

The compression ratio α is defined as the ratio of the magnetic field measured in the probe chamber after compression to the original magnetic field trapped in the flux compressor. If the magnetic flux trapped in the two connected holes in the superconductor is conserved during compression, and if the flux does not penetrate the walls of the superconductor, then an ideal compression ratio α_0 can be calculated from the known dimensions of the two holes and the piston:

$$\alpha_0=\frac{R_1^2+R_2^2}{R_1^2+R_2^2-R_p^2} \tag{3}$$

where R_1 and R_2 are the radii of the compression role and probe hole respectively, and R is the radius of the piston. The flux pump used in the experiment has the dimensions: compression hole 1.650 cm radius, piston 1.610 cm radius, and the probe hole 0.500 cm radius. A compression ratio $\alpha_0=7.94$ is obtained when these dimensions are used in Eq. 3.

Figure 66–7 shows a plot of the experimental compressor ratio α versus the magnetic field compressed into the probe hole. It is observed that a compression ratio of 7.5 is obtained at low fields which compare favorably to the calculated compression ratio α_0. However, at larger fields the compression ratio decreases steadily and is only 2.06 at 23.1 Kg.

It is observed that when the piston is removed from the compression hole the magnetic field returns to approximately the initial value trapped in the two holes. This indicates that the flux does not escape from the compressor. The decrease in compression ratio with increasing magnetic field does indicate that the magnetic flux penetrates a small distance into the walls of the compressor and the piston, and that this penetration is field dependent.

If it is assumed that the magnetic field penetrates a distance δ into the superconducting material, that is

$$B_{int}=B \qquad \delta>r>r_0$$
$$B_{int}=0 \qquad r>\delta \tag{4}$$

where B_{int} is the field in the superconducting material, B is the field compressed in the holes, and r is the distance along the radius of the hole ($r=r_0$ at the interface), then the penetration depth δ and the experimentally measured compression ratio α are related by

$$\alpha=\frac{R_1^2+R_2^2}{R_1^2+R_2^2-R_p^2+\delta^2+2\delta(R_1+R_2+R_p)} \tag{5}$$

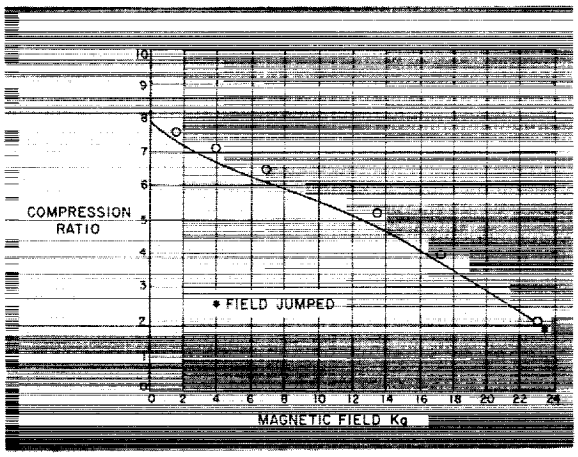

FIGURE 66–7.—A plot of compression ratio of flux compressor vs. compressed magnetic field.

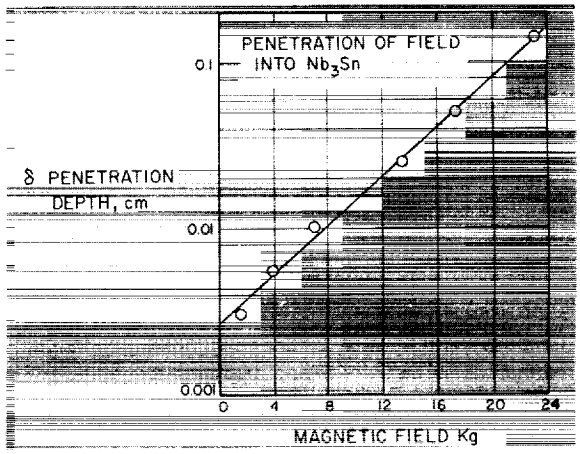

FIGURE 66–8.—A plot of penetration depth in Nb_3Sn vs. magnetic field.

Figure 66–8 shows a plot of the penetration parameter δ computed from Eq. (5) vs. the magnetic field compressed into the probe hole. For the Nb_3Sn used in the experiment the equation

$$\delta(b)=ae^{bB} \tag{6}$$

where $a=2.8\times10^{-3}$ cm and $b = 1.7\times10^{-4}$ gauss^{-1}, gives a good approximation to the experimental data.

REFERENCES

1. KUNZLER, J. E., E. BUEHLER, *F. S. L.* HSU, and J. H. WERNICK, Phys. Rev., Letters *6*, 89 (1961).
2. BERLINCOURT, T. G., R. R. HAKE, *and* D. H. LESLIE, Phys. Rev. Letters *6*, 671 (1961).
3. BERLINCOURT, T. G., R. R. HAKE, Phys. Rev. Letters *9*, 293 (1962).
4. BERLINCOURT, T. G., VIII International Conference on Low Temperature Physics, September 17–21, 1962, London, England.
5. AUTLER, S. H., High Magnetic Fields, MIT Press and John Wiley and Sons, Inc., New York, (1962), p. 324.
6. DONADIEU, L. J., and D. J. ROSE, High Magnetic Fields MIT Press and John Wiley and Sons, Inc., New York (1962), p. 356.
7. HULM, J. K., VIII International Conference on Low Temperature Physics, September 17–21, 1962, London, England.
8. LONDON, F., Superfluids I, John Wiley and Sons, Inc., New York, (1950), p. 27.
9. HILDEBRANDT, A. F., D. D. ELLEMAN, Bull. Am. Phys. Soc. *5*, 111 (1960).
10. HILDEBRANDT, A. F., D. D. ELLEMAN, F. C. WHITMORE, R. SIMPKINS, J. Appl. Phys. *33*, 2375 (1962).
11. ELLEMAN, D. D., A. F. HILDEBRANDT, R. SIMPKINS, F. C. WHITMORE, Bull. Am. Phys. Soc. *7*, 309 (1962).
12. ELLEMAN, D. D., A. F. HILDEBRANDT, JPL Space Program Summary 37–15, *4*, (1962).
13. HILDEBRANDT, A. F., D. D. ELLEMAN, Bull. Am. Phys. Soc. *7*, 473 (1962).